were relatively small and round with few visible neurites. PEMF-mediated neurite outgrowth occurred gradually in a time-dependent manner (Fig. 2B-F). These results indicate that PEMF stimulation has the potential to induce neuritogenesis independently in PC12 cells via an unknown and novel mechanism. Specifically, PEMF-dependent neuritogenesis may involve the activation of an intracellular signaling pathway.

We also assessed whether PEMF exposure increases AChE activity in the cells. Cell lysates were analyzed for AChE activity after culture for 6 or 14 days with exposure to a single PEMF (12 h/day), 50 ng/ml NGF, or 40 ng/ml BMP4. As shown in Fig. 2G, a single PEMF had no significant effect on AChE activity on day 6, in contrast to NGF. However, it significantly increased AChE activity by day 14, similar to BMP4 (Fig. 2H). These results suggest that stimulation with the PEMF gradually induces not only morphological differentiation, but also functional differentiation, in PC12 cells.

Previous work has shown that activation of the ERK1/2 signaling pathway induces neuritogenesis in PC12 cells (Kao *et al.*, 2001) and that NGF-induced ERK1/2 activation and neurite outgrowth are blocked by the MEK1/2 inhibitors PD098059 and U0126 (Ahn and Tolwinski, 1999; Pang *et al.*, 1995). Thus, we next assessed whether PEMF exposure activates the ERK1/2 signaling pathway. Cell lysates were analyzed for endogenous ERK1/2 activity at 20, 60, and 180 min after exposure to a single PEMF in the presence or absence of 2.5 μM U0126. Next, we evaluated the time course of ERK1/2 activity by Western blotting. As shown in Fig. 3A, the induction of ERK1/2 phosphorylation was detected after 60 min of PEMF stimulation and continued up to the 180-min time point. Sustained PEMF-dependent activation of ERK1/2 was completely abolished in the presence of U0126 (Fig. 3A).

We next investigated whether PEMF exposure induces sustained ERK1/2 activation in

other mammalian cells. Cell lysates from either NR8383 cells or PC12 cells (as a control) were analyzed for endogenous ERK1/2 activity at 3 h after stimulation with a single PEMF, a double PEMF (see Materials and Methods for details), or 50 ng/ml NGF (as a positive control). Next, ERK1/2 activity was evaluated by Western blotting. As shown in Fig. 3B, ERK1/2 phosphorylation was detected after 3 h of both PEMF stimulations in PC12 cells, but not NR8383 cells, although it was not as strong as that in NGF-treated cells.

The results presented in Fig. 3 prompted us to determine whether PEMF-mediated activation of the ERK1/2 signaling pathway is required for PEMF-mediated neuritogenesis in PC12 cells. We therefore pretreated cells with the MEK1/2 inhibitor U0126 at a concentration previously shown to abolish PEMF-induced ERK1/2 activation (2.5 μM) (Fig. 3A) prior to the 6-day induction of PEMF-dependent neuritogenesis. The results presented in Fig. 4A-C show that 2.5 μM U0126 almost completely suppressed PEMF-induced neuritogenesis in PC12 cells. We also scored PC12 cells incubated in the presence of U0126 at various concentrations (0-2.5 μM), the other MEK inhibitor PD098059 at a concentration high enough to suppress ERK1/2 activation (10 μM) (Pang *et al.*, 1995), or a negative control for U0126, U0124 (2.5 μM), to assess the inhibition of neurite outgrowth. Our results indicate that U0126 reduced PEMF-mediated neuritogenesis in PC12 cells in a dose-dependent manner (Fig. 4F). In addition, PD098059, but not U0124, also inhibited PEMF-induced neuritogenesis in the cells (Fig. 4D, E, G). These results suggest that PEMF-induced neuritogenesis in PC12 cells requires sustained activation of MEK-ERK1/2 signaling.

Taken together, the results of the present study clearly indicate the essential role of MEK-ERK1/2 signaling in the PEMF-dependent neuronal induction of PC12 cells, and

suggest the existence of a cell type- or cell content-dependent mechanism that mediates PEMF-induced MEK-ERK1/2 signaling. However, how a PEMF induces MEK-ERK1/2 activation and subsequent neuritogenesis in PC12 cells is unclear. In this context, our preliminary data show the TrkA tyrosine kinase inhibitor GW441756 had no significant effect on PEMF-induced neuritogenesis in PC12 cells (data not shown), implying that activation of MEK-ERK1/2 signaling may be independent of TrkA-mediated signaling.

In conclusion, we characterized a novel effect of a PEMF on the differentiation of PC12 cells. Specifically, PEMF exposure can independently induce neuritogenesis through MEK-ERK1/2 activation. Further research into the mechanisms underlying the action of the PEMF and the identification of its critical target signaling molecule(s) leading to neuritogenesis in PC12 cells will promote future application of electromagnetic fields to the regulation of neuronal differentiation.

Acknowledgments. We are grateful to Ms. Ayako Okumoto, Ms. Kanako Tominami, Ms. Shoko Nunome, and Mr. Yoshiyuki Miyamoto for providing technical assistance. This work was supported in part by grants from the Center for Interdisciplinary Research, Tohoku University (Sendai, Japan).

References

Ahn, N.G., and Tolwinski, N.S. 1999. U0126: an inhibitor of MKK/ERK signal transduction in mammalian cells. *Promega Notes*, 71: 4–8.

Deutsch, P.J., and Sun, Y. 1992. The 38-amino acid form of pituitary adenylate cyclase-activating polypeptide stimulates dual signaling cascades in PC12 cells and promotes neurite outgrowth. *J. Biol. Chem.*, 267: 5108–5113.

Fantetti, K.N., and Fekete, D.M. 2012. Members of the BMP, Shh and FGF morphogen families promote chicken statoacoustic ganglion neurite outgrowth and neuron survival in vitro. *Dev. Neurobiol.*, 72: 1213–1228.

Greene, L.A., and Tischler, A.S. 1976. Establishment of a noradrenergic clonal line of rat adrenal pheochromocytoma cells which respond to nerve growth factor. *Proc. Natl. Acad. Sci. USA*, 73: 2424–2428.

Greene, L.A., and Rukenstein, A. 1981. Regulation of acetylcholinesterase activity by nerve growth factor. Role of transcription and dissociation from effects on proliferation and neurite outgrowth. *J. Biol. Chem.*, 256: 6363–6367.

Hayashi, H., Ishisaki, A., Suzuki, M., and Imamura, T. 2001. BMP-2 augments FGF-induced differentiation of PC12 cells through upregulation of FGF receptor-1 expression. *J. Cell Sci.*, 114: 1387–1395.

Heldin, C.H., Miyazono, K., and ten Dijke, P. 1997. TGF-beta signalling from cell membrane to nucleus through SMAD proteins. *Nature*, 390: 465–471.

Hogan, B.L. 1996. Bone morphogenetic proteins in development. *Curr. Opin. Genet. Dev.*, 6: 432–438.

Iwasaki, S., Hattori, A., Sato, M., Tsujimoto, M., and Kohno, M. 1996. Characterization of the bone morphogenetic protein-2 as a neurotrophic factor. Induction of neuronal differentiation of PC12 cells in the absence of mitogen-activated protein kinase activation. *J. Biol. Chem.*, 271: 17360–17365.

Iwasaki, S., Iguchi, M., Watanabe, K., Hoshino, R., Tsujimoto, M., and Kohno, M. 1999. Specific activation of the p38 mitogen-activated protein kinase signaling pathway and induction of neurite outgrowth in PC12 cells by bone morphogenetic protein-2. *J. Biol.*

Chem., 274: 26503–26510.

Kao, S., Jaiswal, R.K., Kolch, W., and Landreth, G.E. 2001. Identification of the mechanisms regulating the differential activation of the MAPK cascade by epidermal growth factor and nerve growth factor in PC12 cells. *J. Biol. Chem.*, 276: 18169–18177.

Kimura, N., Matsuo, R., Shibuya, H., Nakashima, K., and Taga, T. 2000. BMP2-induced apoptosis is mediated by activation of the TAK1-p38 kinase pathway that is negatively regulated by Smad6. *J. Biol. Chem.*, 275: 17647–17652.

Koike, T., Uno, S., Ishizawa, M., Takahashi, H., Ikeda, K., Yokota, S., and Makishima, M. 2006. The heat shock protein inhibitor KNK437 induces neurite outgrowth in PC12 cells. *Neurosci. Lett.*, 410: 212–217.

Kudo, T., Kanetaka, H., Mizuno, K., Ryu, Y., Miyamoto, Y., Nunome, S., Zhang ,Y., Kano, M., Shimizu, Y., and Hayashi, H. 2011. Dorsomorphin stimulates neurite outgrowth in PC12 cells via activation of a protein kinase A-dependent MEK-ERK1/2 signaling pathway. *Genes Cells*, 16: 1121–1132.

Morgado-Valle, C., Verdugo-Díaz, L., García, D.E., Morales-Orozco, C., and Drucker-Colín, R. 1998. The role of voltage-gated Ca2+ channels in neurite growth of cultured chromaffin cells induced by extremely low frequency (ELF) magnetic field stimulation. *Cell Tissue Res.*, 291: 217–230.

Pang, L., Sawada, T., Decker, S.J., and Saltiel, A.R. 1995. Inhibition of MAP kinase kinase blocks the differentiation of PC-12 cells induced by nerve growth factor. *J. Biol. Chem.*, 270: 13585–13588.

Radio, N.M., and Mundy, W.R. 2008. Developmental neurotoxicity testing in vitro: models for assessing chemical effects on neurite outgrowth. *Neurotoxicology*, 29: 361–376.

Rakhit, S., Pyne, S., and Pyne, N.J. 2001. Nerve growth factor stimulation of p42/p44 mitogen-activated protein kinase in PC12 cells: role of G (i/o), G protein-coupled receptor kinase 2, beta-arrestin I, and endocytic processing. *Mol. Pharmacol.*, 60: 63–70.

Rydel, R.E., and Greene, L.A. 1987. Acidic and basic fibroblast growth factors promote stable neurite outgrowth and neuronal differentiation in cultures of PC12 cells. *J. Neurosci.*, 7: 3639–3653.

Schimmelpfeng, J., Weibezahn, K.F., and Dertinger, H. 2005. Neuronal outgrowth of PC-12 cells after combined treatment with nerve growth factor and a magnetic field: influence of the induced electric field strength. *Bioelectromagnetics*, 26: 74–77.

Vaudry, D., Stork, P.J., Lazarovici, P., and Eiden, L.E. 2002. Signaling pathways for PC12 cell differentiation: making the right connections. *Science*, 296: 1648–1649.

Wrana, J.L., Attisano, L., Wieser, R., Ventura, F., and Massague, J. 1994. Mechanism of activation of the TGF-beta receptor. *Nature*, 370: 341–347.

Yanagisawa, M., Nakashima, K., Takeda, K., Ochiai, W., Takizawa, T., Ueno, M., Takizawa, M., Shibuya, H., and Taga, T. 2001. Inhibition of BMP2-induced, TAK1 kinase-mediated neurite outgrowth by Smad6 and Smad7. *Genes Cells*, 6: 1091–1099.

Zhang, Y., Ding, J., and Duan, W. 2006. A study of the effects of flux density and frequency of pulsed electromagnetic field on neurite outgrowth in PC12 cells. *J. Biol. Phys.*, 32: 1–9.

Legends to Figures

Fig. 1. Dose effect of the PEMF on neurite outgrowth in PC12 cells. (A-F) PC12 cells were treated with 40 ng/ml BMP4 or 50 ng/ml NGF, exposed to a single PEMF (sPEMF) for various time periods, or left untreated for 6 days. Phase-contrast images of PC12 cells on day 6 after culture without stimulation (A), with PEMF exposure for 0.75 h/day (B), with PEMF exposure for 3 h/day (C), with PEMF exposure for 12 h/day (D), with 40 ng/ml BMP4 (E), or with 50 ng/ml NGF (F). Scale bar, 100 μm. Similar results were obtained in three independent experiments. (G, H) PC12 cells were treated with 40 ng/ml BMP4 or 50 ng/ml NGF, exposed to the PEMF for the indicated time periods, or left untreated for 6 days, and the percentage of neurite-bearing cells on day 6 was determined. The data represent the mean ± SE of three replicates. $^{**}P < 0.01$ vs. the day-6 controls with no stimulation.

Fig. 2. Time course of PEMF-induced neuronal differentiation in PC12 cells. (A-E) PC12 cells were exposed to a single PEMF (sPEMF) for a 12-h period each day or left untreated for 7 days. (A) Phase-contrast images of the cells on day 0 prior to exposure to the PEMF. Phase-contrast image of PC12 cells on day 3 after exposure to the PEMF (12 h/day) (B) or no stimulation (C). Phase-contrast image of PC12 cells on day 7 after exposure to the PEMF (12 h/day) (D) or no stimulation (E). Scale bar, 100 μm. Similar results were obtained in three independent experiments. (F) PC12 cells were exposed to the PEMF for 12 h/day or left untreated for 7 days, and the percentage of neurite-bearing cells on days 0, 1, 3, and 7 was determined. The data represent the mean ± SE of three replicates. $^{*}P < 0.05$, $^{**}P < 0.01$ vs. the day 0 control with no treatment. (G, H) Cell lysates from PC12 cells were prepared and analyzed for acetylcholine esterase (AChE) activity after stimulation with a sPEMF (12 h/day) or positive controls (50 ng/ml NGF or 40 ng/ml BMP4) for the indicated periods of time. The data represent the mean ± SE of three replicates. $\dagger\dagger P < 0.01$ vs. the day-0 control with no stimulation. n.s., not significant vs. the day 0 control with no treatment. $^{**}P < 0.01$ vs. the day-6 or day-14 control with no stimulation.

Fig. 3. Sustained PEMF-induced activation of endogenous ERK1/2 in PC12 cells. (A) PC12 cells were exposed to a single PEMF (sPEMF) for 20, 60, or 180 min or left untreated in the presence or absence of the MEK1/2 inhibitor U0126 (2.5 μM). Equal amounts of the sample proteins were immunoblotted and probed with antibodies against phosphorylated (activated) ERK1/2 (p-ERK1/2) and ERK1/2. (B) PC12 or NR8383 cells were exposed to a sPEMF or a double PEMF (dPEMF), treated with 50 ng/ml NGF (as a positive control), or left untreated for 3 h. Equal amounts of the sample proteins were immunoblotted and probed with antibodies against p-ERK1/2 and ERK1/2. Representative blots are shown. Similar results were obtained in three independent experiments. IB, immunoblot.

Fig. 4. Suppression of PEMF-induced neurite outgrowth in PC12 cells by MEK1/2 inhibitors. (A-E) PC12 cells were exposed to a single PEMF (12 h/day) or left untreated for 6 days in the presence of 2.5 μM U0126, 2.5 μM U0124, or 10 μM PD098059. Representative phase-contrast images of PC12 cells on day 6 after culture with no stimulation (A), the PEMF (12 h/day) (B), the PEMF (12 h/day) plus 2.5 μM U0126 (C), the PEMF (12 h/day) plus 2.5 μM U0124 (D), or the PEMF (12 h/day) plus 10 μM

PD098059 (E). Scale bar, 100 μm. Similar results were obtained in three independent experiments. (F, G) PC12 cells were exposed to the PEMF (12 h/day) or left untreated for 6 days in the presence of the indicated concentrations of U0126, U0124, and PD098059. The percentage of neurite-bearing cells on day 6 was assayed. The data represent the mean ± SE of three replicates. ††$P < 0.01$ vs. the day 0 control with no stimulation. **$P <$ 0.01 vs. PEMF stimulation (12 h/day) alone on day 6. n.s., not significant vs. PEMF stimulation (12 h/day) alone on day 6. PD, PD098059.

Fig. 1 **Kudo *et al.***

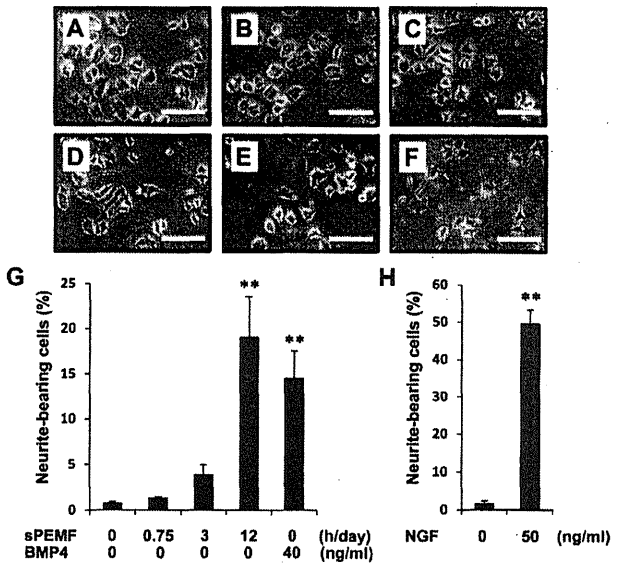

Fig. 2 Kudo *et al.*

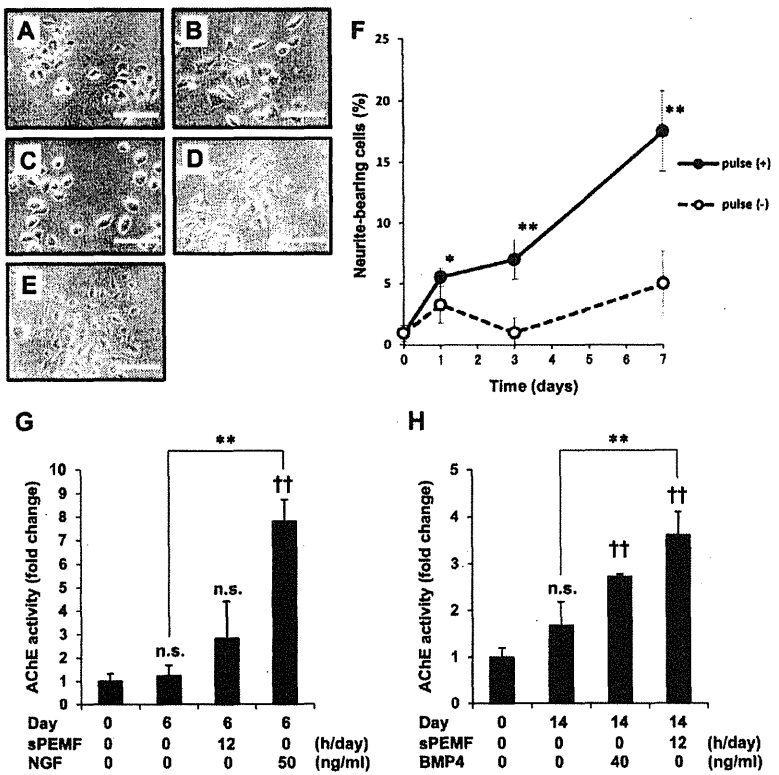

Fig. 3 Kudo *et al.*

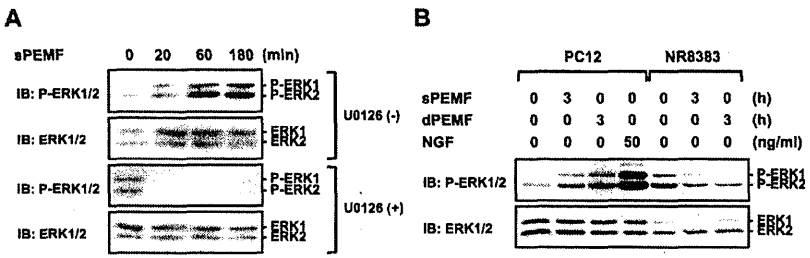

Fig. 4

Kudo *et al.*

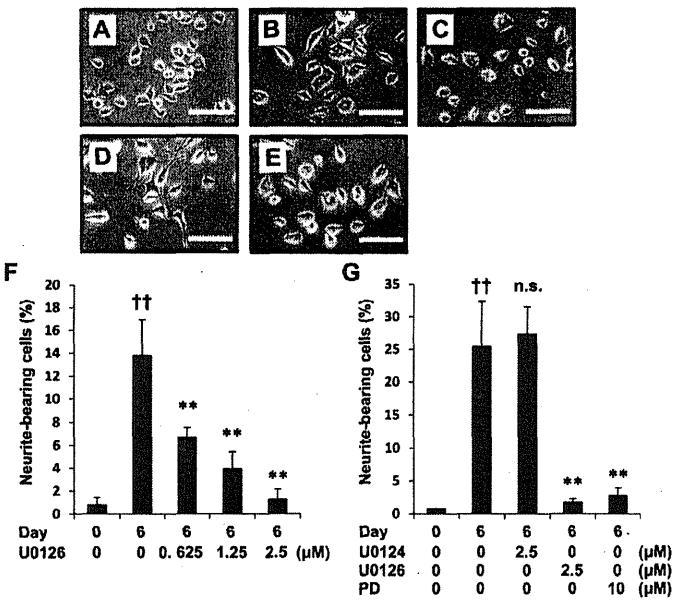

Japanese Journal of Applied Physics 50 (2011) 07HA01 **REVIEW PAPER**
DOI: 10.1143/JJAP.50.07HA01

Minute Mechanical-Excitation Wave-Front Propagation in Human Myocardial Tissue

Hiroshi Kanai* and Motonao Tanaka[1]

Graduate Schools of Biomedical Engineering and Engineering, Tohoku University, Sendai 980-8579, Japan
[1]*Cardiovascular Center, Tohoku Welfare Pension Hospital, Sendai 983-0005, Japan*

Received January 18, 2011; accepted March 9, 2011; published online July 20, 2011

Complexity of the cardiac contraction sequence is still not fully understood because the dynamic *mechanical excitation* process, which directly correlates with contraction, cannot be accurately measured based on the electro-magnetic phenomena. By developing a noninvasive novel imaging modality with high temporal and spatial resolutions, the present study shows that the propagation of the mechanical wave-front occurs at the beginning of cardiac contraction sequence for the first time (about 60 ms prior to the ordinarily accepted onset time of the contraction). From the apical side of the interventricular septum, a minute velocity component with an amplitude of several tenth micrometers is generated and it propagates from the apex to the base of the posterior wall, and then from the base to the apex of the septum, with a propagation speed of 3–9 m/s. This dynamic measurement modality is also applicable to various tissues in biology. © 2011 The Japan Society of Applied Physics

1. Introduction

Unlike the case of skeletal muscle, the direction of myocardial contraction does not coincide with the direction of work necessary to eject the intraventricular blood, contributing to great complexity of the wall deformation sequence of cardiac contraction. Electrocardiography is an invaluable clinical tool for the diagnosis of cardiac failure. Electrocardiographic measurement[1)] has realized noninvasive imaging of the spatial distribution of action potentials, and magnetocardiography[2)] conducted inside a shielded room enables similar imaging. By these electro-magnetic phenomena-based methods, however, *mechanical properties* of myocardial velocity and contraction are not been directly measured. Other cardiac imaging tools, namely, computed tomography (CT),[3)] magnetic resonance imaging (MRI),[4,5)] single photon emission computed tomography (SPECT),[6)] and conventional echocardiography,[7,8)] enable visualization of two-dimensional (2D) or three-dimensional (3D) images, motion, torsional deformation, asynchronous wall motion during acute myocardial ischemia,[9)] and the left ventricular inflow.[10)] The time of peak contraction of the heart wall has been reported using 3D MRI tagging.[11)] With MRI tagging, the onset time of the contraction has been reported.[12,13)] However, their visualization is restricted to static configurations or *large* and *slow* motion due to contraction. Using the Doppler effect of the ultrasound, the velocity or displacement are measured,[14,15)] but an accurate waveform for which the frequency analysis is applicable is not obtained, and measurement of minute, rapid velocity waveforms at the beginning of the contraction in the heart wall has not been attempted.

We have previously found that the rapid response of the excised heart muscle of a rat to electrical stimulations is minute (displacement of 30 μm and velocity of 0.5 mm/s)[16)] and that *velocity measurement* is superior to *displacement measurement* since the displacement is the accumulation of velocity, that is, low-pass filtering.[17)] To realize *noninvasive* detection of such minute mechanical responses to the propagation of the action potential in the human heart, we developed a novel ultrasound-based noninvasive method[18)] and we successfully measured such response as a velocity waveform for human subjects for the first time.[19)] In the present study, the regional change in length or wall thickness was simultaneously measured with high temporal resolution to confirm whether the detected velocity component corresponds to the myocardial contraction or extension.

2. Materials and Methods

In the present study, the minute propagation of the contraction/relaxation was visualized for the first time in the human as follows: The ultrasonic beams transmitted by the ultrasound probe attached to the chest wall scan the 2D plane of the heart, and the RF reflective wave for each ultrasound transmission is acquired by the same probe as in conventional echocardiography. In this novel method, however, the phase shift between the succeedingly acquired RF signals in the same direction is determined accurately at each point in the heart wall along the ultrasonic beam, and the position of each point is tracked. Thus, the minute motion at each point is measured as a velocity waveform so that the Fourier transform is applicable.[17,20)] The six periods (atriosystolic phase, isovolumetric contraction period, ejection period, isovolumetric relaxation phase, period of rapid filling, and period of slow filling) during one cardiac cycle were characterized by the measured waveforms.[21)] Moreover, by restricting the number of directions of transmission to maintain a high frame rate (500 Hz), the velocity waveforms are simultaneously obtained at about 3,000 points set in the heart wall on the 2D plane.[22)] Spatial distribution of the heart wall vibrations generated by remote perturbation of the inner pressure was also noninvasively measured by the method.[23)] By applying frequency analysis to each velocity waveform,[17)] the phase of its 40-Hz component is detected and its instantaneous 2D distribution is reconstructed at every 2 ms, precisely revealing the minute-wave propagation in the heart wall[22)] by neglecting the differences in the amplitude components. The achieved lower limit in the velocity measurement has been validated as being 0.1 mm/s,[20)] which corresponds to 0.2 μm in displacement during 2 ms. Since the wavelength is about 410 μm for the typical frequency (3.75 MHz), 0.2 μm corresponds to about 1/2000 of the wavelength. Such a minute velocity component superimposed on the large motion due to heartbeat cannot be noninvasively measured by any other known method. At the same time, the regional change in length of thickness is accurately obtained from the spatial difference between the velocity waveform at the adjacent points (820 μm apart) with 0.5-μm accuracy.[24)] The propagation of the contraction in the heart wall was detected just at the apical side of the interventricular septum.[25)]

*E-mail address: kanai@ecei.tohoku.ac.jp

Person-to-person distribution (up to 10 persons) by the author only. Not permitted for publication for institutional repositories or on personal Web sites.

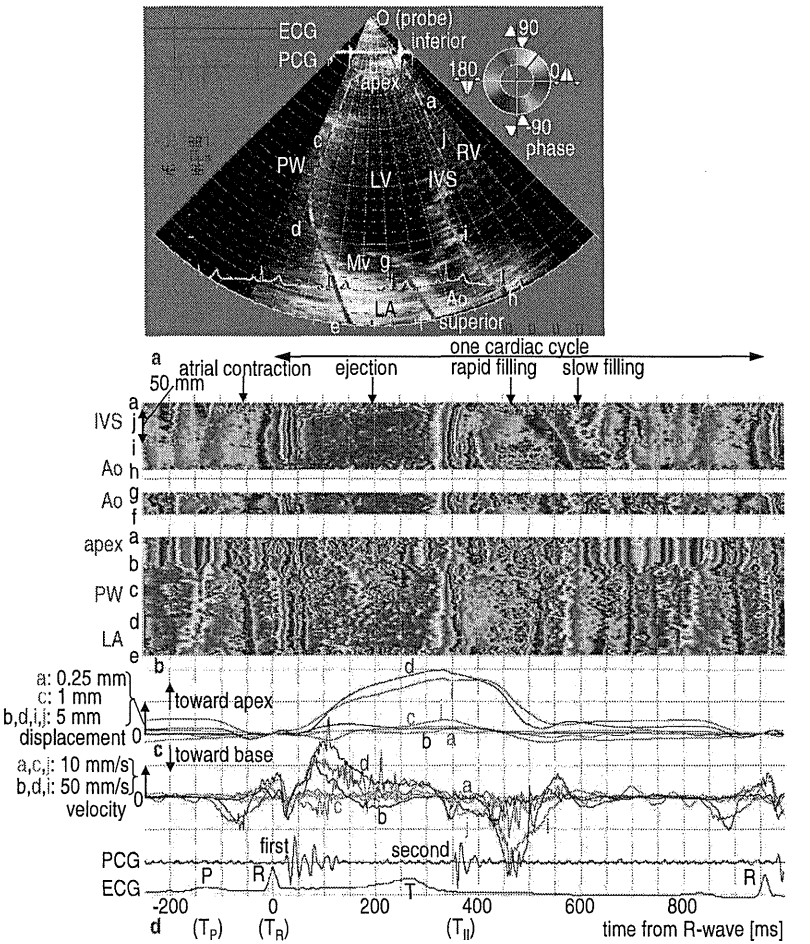

Fig. 1. (Color online) Time sequence of velocity and displacement in the unfolded left ventricular wall based on the apical view. (a) Cross-sectional image from apical view of the LV of a healthy young subject. The two colored lines passing through the walls show the phase of the 40-Hz component of the velocity wave at each point at T_R. Red and light blue correspond to the upward and downward movements, respectively. (b) Temporal changes in the phase of 40-Hz component of the velocity wave for one cardiac cycle along the two lines in (a). Vertical axis corresponds to the line in (a). (c) Displacement waveform at points a–j in (a). (d) Velocity waveform at points a–j with electrocardiogram (ECG) and phonocardiogram (PCG). (Ao = aortic valve; LA = left atrium; Mv = mitral valve; RV = right ventricle; PW = posterior wall.)

3. *In vivo* Experimental Results

By applying this novel method to the longitudinal-sectional plane of a healthy human heart as shown in Fig. 1(a), the velocity signal was measured as a waveform at each point on the plane. The velocity waveforms measured at six points (a–j) in Fig. 1(a) and their integration, the displacement waveform, are shown in Figs. 1(d) and 1(c), respectively, for one cardiac cycle. The left ventricular (LV) contraction during the ejection period is roughly shown in the upward displacement (toward the apex) of Fig. 1(c). In the velocity waveform of Fig. 1(d), from the time of the P-wave, T_P, of the

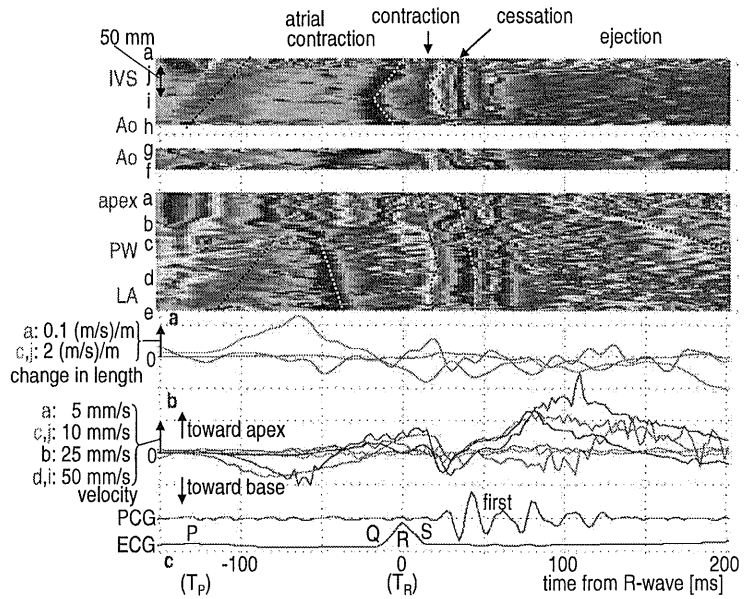

Fig. 2. (Color online) Expanded version of Fig. 1 at the beginning of the contraction. (a) Temporal changes in the phase of the 40-Hz component of the velocity wave in Fig. 1(b). (b) Temporal changes in thickness or length at points a–j in Fig. 1(d). (c) Velocity waveform at points a–j.

electrocardiography, there is downward velocity component (toward the base), corresponding to the LV expansion due to atrial contraction. After this, during systole, the upward velocity component (toward the apex) begins, which corresponds to the LV contraction, continuing until the time of the second heart sound, T_{II}, the time of the aortic valve closure, which is followed by rapid filling and slow filling phases, where these points moves downward (toward the base).

However, there are some differences among these transient times from downward to upward or from upward to downward at the base-side points (d or i). To clearly show these time differences regardless of the minuteness of the velocity, by applying the moving short-time Fourier transform to each of the velocity waveforms, simultaneously measured at all points set along the lines (a–b–c–d–e, g–f, and a–j–i–h) in Fig. 1(a), the phase of the 40-Hz component is color-coded, and its temporal change is shown in Fig. 1(b). Red shows the upward velocity component toward the probe (point O) in Fig. 1(a), and light blue shows its reverse property. As shown in Fig. 1(b), the onset time of the upward velocity (contraction) before time of R-wave of the electrocardiography, T_R, does not coincide at all points (a–j), but there are some propagating components in the LV.

By expanding the time axis in Figs. 1(b) and 1(d), the transition properties around T_R are shown in Figs. 2(a) and 2(c), respectively. At the same time, the instantaneous change in length (shortening due to contraction or extension) is obtained at the points (a, c, j) shown in Fig. 2(b). The white dotted lines in Fig. 2(a) show the onset of the contraction determined by confirming whether the red component of velocity is associated with the change in length from extension to contraction as in Fig. 2(b). The black dotted lines show the reverse phenomenon.

From T_P, the atrial contraction begins and the LV volume increases, corresponding to the downward velocity (light green) in Fig. 2(a) to show the extension both in the posterior wall (b–c–d) and the interventricular septum (IVS) (a–j–i). Then, from the time 80 ms prior to T_R, the upward velocity component is generated at the apical side (a), and then from the time of 50 ms prior to T_R, the upward component propagates from the apex (b) to the base (e) along the LV posterior wall with a speed of about 9 m/s, where it is accompanied by the transition from extension to contraction. It then propagates along the IVS from point (i) to both the apex (a) and the base (h) at a speed of about 3 m/s. Just after passage of this component, the contraction begins at each point. The starting point (a) of the velocity component accompanying the contraction in Fig. 2(a) would be close to the terminal of the Purkinje fibers (special electrical conducting cells which rapidly transmit an electrical excitation).[26] These velocity and change in length are too minute to be identified by other methods.

Person-to-person distribution (up to 10 persons) by the author only. Not permitted for publication for institutional repositories or on personal Web sites.

Jpn. J. Appl. Phys. **50** (2011) 07HA01 **REVIEW PAPER**

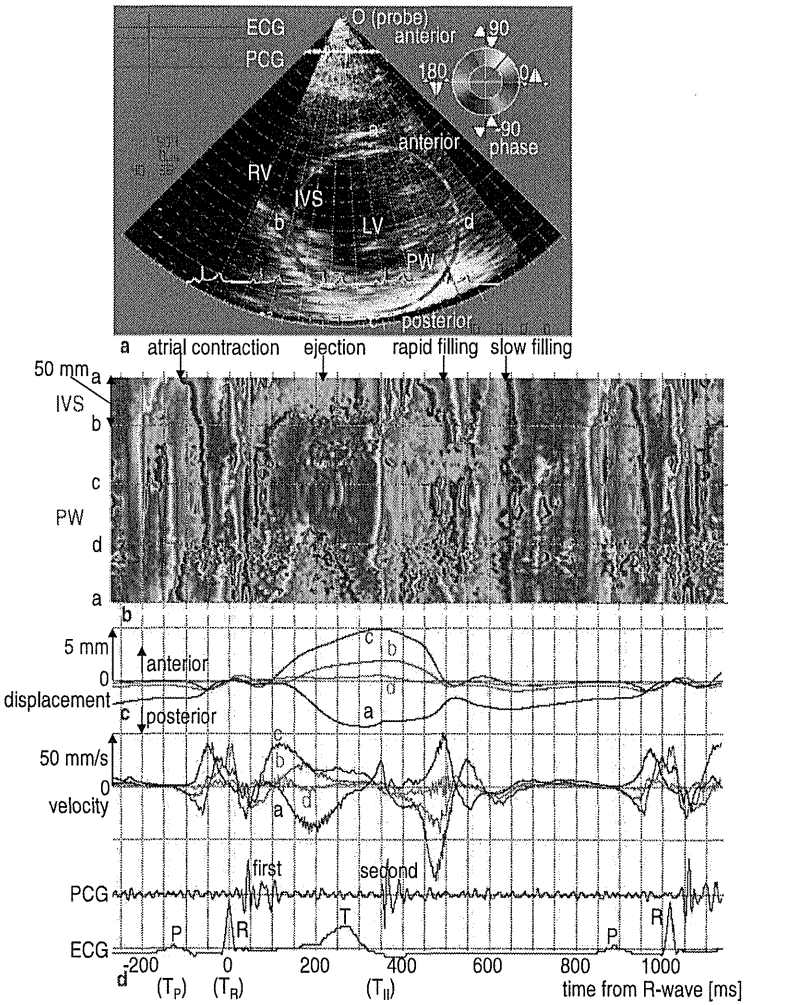

Fig. 3. (Color online) Time sequence of velocity and displacement in the unfolded left ventricular wall made based on the short-axis view. (a) Short-axis cross-sectional plane on the LV with the papillary muscle level. (b) For one cardiac cycle, the temporal changes in the phase of the velocity component. Vertical axis corresponds to the colored line in (a). (c) Displacement waveform at points a–d in (a). (d) Velocity waveform at points a–d.

The first heart sound following the QRS-complex is traditionally thought to be primarily associated with mechanical vibrations resulting from the closure of the mitral value and the opening of the aortic valve.[27] As shown in Fig. 2(a), after T_R, two waves are generated and propagate from the apex (a) to the base (e) along the LV posterior wall. During the short period of 20 ms from the beginning of the first heart sound, the contraction property, which begins at the above onset in Fig. 2(a), is reversed. This "cessation of the contraction" would correspond to the LV expansion

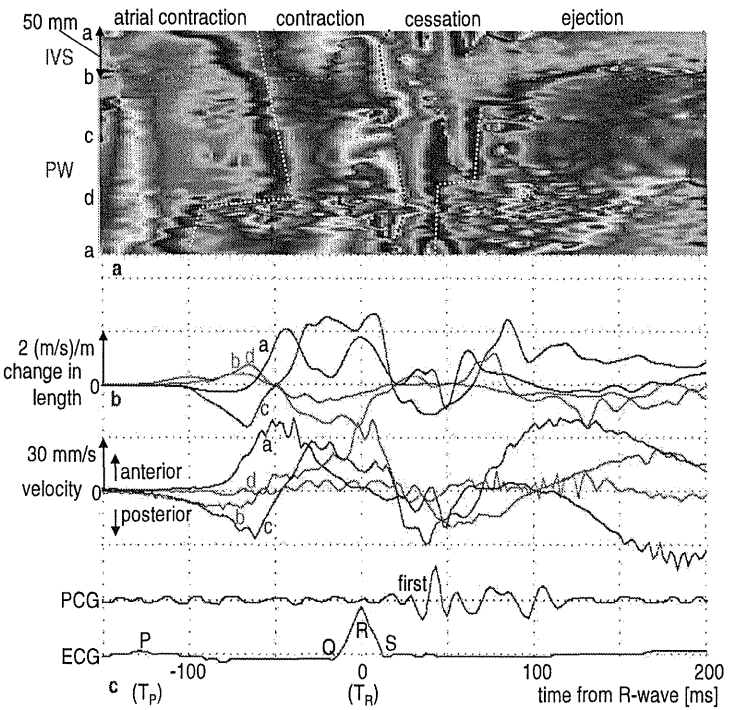

Fig. 4. (Color online) Expanded version of Fig. 3 at the beginning of the contraction. (a) Temporal changes in the phase of the velocity component in Fig. 3(b). (b) Typical waveforms of the change in thickness at point c and change in length at point b. (c) Velocity waveform measured at points a–d.

in the pre-ejection period that is necessary to cause the mitral valve closure.[28] This cessation is terminated by the beginning of the second component of the above two waves, and after this cessation, all the points have the upward velocity components [red in Fig. 2(a)], that is, the contraction restarts, which constitutes the substantial LV contraction in the ejection period.

For the same subject, the position and the direction of the ultrasonic probe are changed so that the velocity and change in thickness are measured in the parasternal short-axis cross-sectional plane of the LV, as shown in Fig. 3(a). Figures 3(d) and 3(b) respectively show the velocity waveforms at four points (a–b–c–d) in Fig. 3(a) and temporal changes in the phase of the velocity waveform for one cardiac cycle. Figure 3(c) shows the displacement waveforms at these points. Roughly, during the ejection period, the LV contraction is associated with the downward displacement (to posterior) at point (a) and upward displacement (to anterior) at points (b, c), while point (d) is almost motionless.

By expanding the time axis in Fig. 3, the mechanical excitation is shown in Fig. 4 around T_R. From a time 120 ms prior to T_R, the response propagates from the IVS (a), to the posterior wall (b–c–d) with a speed of about 6 m/s in the counterclockwise direction when viewed from the apical side. The propagation is *unidirectional*, that is, the contraction propagates in one direction (counterclockwise), not in both directions. The passage of the component [blue in Fig. 4(a)] is accompanied by thickening (at a and c) or contraction (at b and d) along the ultrasonic beam; both correspond to the contraction.

4. Discussion

Previous studies have defined the pre-ejection period[28,29] as the interval from the onset of the QRS-complex to the time of the aortic valve opening. It has been shown that myocardial acceleration during isovolumic contraction (IVA), which onset coincides with the initial upstroke of the LV pressure and the R-wave of the ECG, is clinically useful to measure LV contractile function that is unaffected by preload and afterload changes.[30,31] The importance of the present study is not to measure the pre-contraction or the IVA but to measure the spatial and temporal distribution of the onsets of the IVA to show its excitation propagation. The end of the cessation in Figs. 2(a) and 4(a) corresponds to the traditionally accepted onset time of the contraction.[12,13] However, the minute contraction propagation occurring prior to the onset time was found in the present study. Physiologically, it is well known that the depolarized action potentials, cyclically generated at the sino-atrial node, propagate to the Purkinje fibers, which form interweaving networks on the endocardial surface of both ventricles and transmit the impulse to the ventricular endocardium. Their conduction velocity is 2.0–4.0 m/s in the normal human.[32,33] Around the time of the Q-wave, based on cell-to-cell connections, the action potential starts to propagate with a lower speed of 0.3–1.0 m/s in humans[33] to the entire wall from the Purkinje fiber-myocyte junctions on the IVS surface, where the Purkinje fibers are in contact with the myocardium. In the present study, however, the measured propagation velocity regarding the minute contraction is about 9 m/s, which is much faster than those electrical conduction velocities in the previous studies. These differences suggest that the measured propagation components prior to T_R would be "pre-contraction" prior to the full contraction of the ejection period. Since the physiological basis of the observed contraction sequence remains unclear, further mechanistic details will be necessary to better substantiate these findings.

In the present study, the heart walls were manually identified before applying the measurement method. For applying the analysis in the present study to a lot of subjects and animals, it is essential to develop a reliable method for the automated identification of the heart wall.[34–37]

In the present study, the measurement of the velocity components was restricted to the direction of the ultrasonic beam. Alternatively, the measurement has been expanded into the two-dimensional (2D) space recently.[38–41] It is, however, still difficult to measure the rapid and minute velocity components in the heart wall by these methods. For thorough analysis of the propagation of the minute mechanical-excitation wave-front, the heart wall velocity distribution should be measured in the 2D space with high temporal and spatial resolutions.[42]

With the novel echocardiography in the present study, the minute-contraction sequences of the myocardium were confirmed noninvasively. These results show great potential for thorough understanding of the principles of the cardiac contraction mechanism, as well as for noninvasive assessment of myocardial tissue damage in early stage of cardiomyopathy and myocardial infarction since it is known that myocardial isotonic velocity for the contraction is decreased in failing hearts.[43] The biological implications of these observations also remain unclear. In order to elucidate the role of these contractions in the ventricular remodeling, similar experiments should be performed in infracted hearts. Moreover, investigation of methods to modulate these contractions should be performed to determine any potential therapeutic value with biventricular pacing.

Acknowledgments

The authors wish to thank Dr. Hideyuki Hasegawa of Tohoku University for experimental contributions. The study was approved by the review committee of the Graduate School of Engineering, Tohoku University and the healthy subjects gave informed consent. This study was partly supported by a Grant-in-Aid for Scientific Research from the Japan Society for the Promotion of Science (2008–2010, No. 20360181).

1) C. Ramanathan, R. N. Ghanem, P. Jia, K. Ryu, and Y. Rudy: Nat. Med. **10** (2004) 422.
2) R. A. Stratbucker, C. M. Hyde, and S. E. Wixson: IEEE Trans. Bio-Med. Electron. **10** (1963) 145.
3) L. T. Mahoney, W. Smith, M. P. Noel, M. Florentine, D. J. Skorton, and S. M. Collins: Invest. Radiol. **22** (1987) 451.
4) L. Axel and L. Dougherty: Radiology **171** (1989) 841.
5) M. B. Buchalter, J. L. Weiss, W. J. Rogers, E. A. Zerhouni, M. L. Weisfeldt, R. Beyar, and E. P. Shapiro: Circulation **81** (1990) 1236.
6) A. Wagner, H. Mahrholdt, T. A. Holly, M. D. Elliott, M. Regenfus, M. Parker, F. J. Klocke, R. O. Bonow, R. J. Kim, and R. M. Judd: Lancet **361** (2003) 374.
7) Y. Notomi, R. M. Setser, T. Shiota, M. G. Martin-Miklovic, J. A. Weaver, Z. B. Popovic, H. Yamada, N. L. Greenberg, R. D. White, and J. D. Thomas: Circulation **111** (2005) 1141.
8) G. R. Sutherland, M. J. Stewart, K. W. Groundstroem, C. M. Moran, A. Fleming, F. J. Guell-Peris, R. A. Riemersma, L. N. Fenn, K. A. Fox, and W. N. McDicken: J. Am. Soc. Echocardiogr. **7** (1994) 441.
9) C. Pislaru, M. Belohlavek, R. Y. Bae, T. P. Abraham, J. F. Greenleaf, and J. B. Seward: J. Am. Coll. Cardiol. **37** (2001) 1141.
10) M. J. Garcia, J. D. Thomas, and A. L. Klein: J. Am. Coll. Cardiol. **32** (1998) 865.
11) C. G. Fonseca, H. C. Oxenham, B. R. Cowan, C. J. Occleshaw, and A. A. Young: Am. J. Physiol. Heart Circ. Physiol. **285** (2003) H621.
12) B. T. Wyman, W. C. Hunter, F. W. Prinzen, and E. R. McVeigh: Am. J. Physiol. Heart Circ. Physiol. **276** (1999) H881.
13) J. J. M. Zwanenburg, M. J. W. Götte, J. P. A. Kuijer, R. M. Heethaar, A. C. van Rossum, and J. T. Marcus: Am. J. Physiol. Heart Circ. Physiol. **286** (2004) 1872.
14) J. J. Bax, T. A. Abraham, S. S. Barold, O. A. Breithardt, J. W. H. Fung, S. Garrigue, J. Gorcsan III, D. L. Hayes, D. A. Kass, J. Knuuti, C. Leclercq, C. Linde, D. B. Mark, M. J. Monaghan, P. Nihoyannopoulos, M. J. Schalij, C. Stellbrink, and C.-M. Yu: J. Am. Coll. Cardiol. **46** (2005) 2168.
15) K. Miyatake, M. Yamagishi, N. Tanaka, M. Uematsu, N. Yamazaki, Y. Mine, A. Sano, and M. Hirama: J. Am. Coll. Cardiol. **25** (1995) 717.
16) H. Kanai, S. Katsumata, H. Honda, and Y. Koiwa: Acoust. Sci. Technol. **24** (2003) 17.
17) H. Kanai, M. Sato, N. Chubachi, and Y. Koiwa: IEEE Trans. Ultrason. Ferroelectr. Freq. Control **43** (1996) 791.
18) H. Kanai: IEEE Trans. Ultrason. Ferroelectr. Freq. Control **52** (2005) 1931.
19) H. Kanai: Ultrasound Med. Biol. **35** (2009) 936.
20) H. Kanai, H. Hasegawa, N. Chubachi, Y. Koiwa, and M. Tanaka: IEEE Trans. Ultrason. Ferroelectr. Freq. Control **44** (1997) 752.
21) H. Kanai, Y. Koiwa, Y. Saito, I. Susukida, and M. Tanaka: Jpn. J. Appl. Phys. **38** (1999) 3403.
22) H. Kanai and Y. Koiwa: Ultrasound Med. Biol. **27** (2001) 481.
23) H. Kanai, H. Hasegawa, and K. Imamura: Jpn. J. Appl. Phys. **45** (2006) 4718.
24) H. Kanai, K. Sugimura, Y. Koiwa, and Y. Tsukahara: Electron. Lett. **35** (1999) 949.
25) H. Yoshiara, H. Hasegawa, H. Kanai, and M. Tanaka: Jpn. J. Appl. Phys. **46** (2007) 4889.
26) F. H. Netter: *A Compilation of Paintings on the Normal and Pathologic Anatomy and Physiology, Embryology, and Diseases of the Heart* (Ciba Pharmaceutical, Summit, 1969).
27) A. A. Luisada and F. Portaluppi: *The Heart Sounds: New Facts and Their Clinical Implications* (Praeger Scientific, New York, 1982).
28) E. W. Remme, E. Lyseggen, T. Helle-Valle, A. Opdahl, E. Pettersen, T. Vartdal, A. Ragnarsson, M. Ljosland, H. Ihlen, T. Edvardsen, and O. A. Smiseth: Circulation **118** (2008) 373.
29) A. M. Weissler, W. S. Harris, and C. D. Schoenfeld: Circulation **37** (1968) 149.
30) M. Vogel, M. M. H. Cheung, J. Li, S. B. Kristiansen, M. R. Schmidt, P. A. White, K. Sorensen, and A. N. Redington: Circulation **107** (2003) 1647.
31) E. Lyseggen, S. I. Rabben, H. Skulstad, S. Urheim, C. Risoe, and O. A. Smiseth: Circulation **111** (2005) 1362.
32) D. Durrer, R. T. van Dam, G. E. Freud, M. J. Janse, F. L. Meuler, and R. C. Arzbaecher: Circulation **41** (1970) 899.

Person-to-person distribution (up to 10 persons) by the author only. Not permitted for publication for institutional repositories or on personal Web sites.

Jpn. J. Appl. Phys. **50** (2011) 07HA01 **REVIEW PAPER**

33) A. M. Katz: *Physiology of the Heart* (Lippincott Williams & Wilkins, Philadelphia, PA, 2001) 3rd ed., p. 518.
34) T. Kinugawa, H. Hasegawa, and H. Kanai: Jpn. J. Appl. Phys. **47** (2008) 4155.
35) R. J. Watson, C. C. McLean, M. P. Moore, T. Spencer, D. M. Salter, T. Anderson, K. A. A. Fox, and W. N. McDicken: Ultrasound Med. Biol. **26** (2000) 73.
36) K. R. Waters, S. L. Bridal, C. Cohen-Bacrie, C. Levrier, P. Fornès, and P. Laugier: Ultrasound Med. Biol. **29** (2003) 1521.
37) C. S. Hall, E. D. Verdonk, S. A. Wickline, J. E. Perez, and J. G. Miller: J. Acoust. Soc. Am. **101** (1997) 563.
38) L. N. Bohs, B. J. Geiman, M. E. Anderson, S. C. Gebhart, and G. E. Trahey: Ultrasonics **38** (2000) 369.
39) S. Langeland, J. D'hooge, H. Torp, B. Bijnens, and P. Suetens: Ultrasound Med. Biol. **29** (2003) 1177.
40) S. Langeland, J. D'hooge, T. Claessens, P. Claus, P. Verdonck, P. Suetens, G. R. Sutherland, and B. Bijnens: IEEE Trans. Ultrason. Ferroelectr. Freq. Control **51** (2004) 1537.
41) N. Nitta and T. Shiina: Jpn. J. Appl. Phys. **43** (2004) 3249.
42) Y. Honjo, H. Hasegawa, and H. Kanai: Jpn. J. Appl. Phys. **49** (2010) 07HF04.
43) J. F. Spann, Jr., R. A. Buccino, E. H. Sonnenblick, and E. Braunwald: Circ. Res. **21** (1967) 341.

International Journal of Cardiology xxx (2012) xxx–xxx

Contents lists available at SciVerse ScienceDirect

International Journal of Cardiology

journal homepage: www.elsevier.com/locate/ijcard

Letter to the editor

Longitudinal changes in the relationship between serum adiponectin concentration and cardiovascular risk factors among apparently healthy middle-aged adults ☆

Kaijun Niu [a,b,*], Yoritoshi Kobayashi [b], Lei Guan [b], Haruki Momma [b], Hui Guo [b], Yufei Cui [b], Atsushi Otomo [b], Masahiko Chujo [b], Ryoichi Nagatomi [b]

[a] Department of Nutrition and Food Hygiene, School of Public Health, Tianjin Medical University, Tianjin, People's Republic of China
[b] Division of Biomedical Engineering for Health & Welfare, Tohoku University Graduate School of Biomedical Engineering, Sendai, Japan

ARTICLE INFO

Article history:
Received 21 October 2012
Accepted 1 November 2012
Available online xxxx

Keywords:
Adiponectin
Cardiovascular disease risk factors
Longitudinal study

Cumulative evidence from experimental and clinical studies suggests that adiponectin plays a protective role in the cardiovascular system [1]. However, surprisingly, several longitudinal studies have indicated that adiponectin increased with age [2,3], and that a higher longitudinal increase in adiponectin predicted increased mortality in older persons [2,3]. Furthermore, several prospective cohort studies have also indicated that higher baseline levels of adiponectin were related with increased all-cause and cardiovascular disease (CVD) mortality, and with the severity of congestive heart failure [4,5]. Thus, the exact role of increased adiponectin production under pathophysiological conditions has not yet been fully identified [4,5].

In order to investigate whether the increase in adiponectin with age has a beneficial or detrimental effect on CVD, we considered that investigating how the change in adiponectin is related with the changes in well-recognized risk factors for CVD among populations with different age or health statuses may be the key. We therefore designed a 3-year longitudinal study to investigate how the change in adiponectin is related with the changes in well-recognized risk factors for CVD among apparently healthy middle-aged adults.

The Oroshisho longitudinal study was composed of a longitudinal cohort of adult employees working at the Sendai Oroshisho Center, in Sendai, Northern Japan. A detailed description of the methods has been published elsewhere [6]. In 2008, there were 1253 individuals, who had a received health examination; of these, 1154 individuals agreed to participate and provided informed consent for their data to be analyzed. The 3-year follow-up data were analyzed in the longitudinal study. The Institutional Review Board of the Tohoku University Graduate School of Medicine approved the study protocol. Participants were excluded at baseline if they did not have adiponectin or high-sensitive C-reactive protein (hsCRP) ($n=21$); if they had a history of CVD ($n=12$). Of those invited, 141 subjects did not undergo health examinations during follow up, and the data from 980 subjects were used.

All statistical analyses were performed using the Statistical Analysis System 9.3 edition (SAS Institute Inc., Cary, NC, USA). Analysis of covariance (ANCOVA) was used to examine the relationships between the sex-specific quartiles of the adiponectin change and the change of the CVD risk factors during the follow-up period, after adjustment for covariates. All tests were 2-tailed, and $p<0.05$ was defined as statistically significant.

Age-adjusted baseline characteristics according to the sex-specific tertiles of adiponectin change over the 2-year follow up period are shown in Table 1. Compared to individuals in the lowest and/or middle category groups, the highest tertiles of adiponectin change had lower body mass index (BMI) and, triglycerides (TG), with the highest tertile having higher levels of high-density lipoprotein cholesterol (HDL), and adiponectin ($p\leq0.001$). A significantly larger percentage of high PA was observed in the highest category of adiponectin change when compared to the middle tertile ($p<0.01$). Other than these results, no significant differences were observed between the categories of adiponectin change. Similar baseline characteristics were also observed in the sex-specific tertiles of adiponectin change at the 1-year follow up (data not shown).

The adjusted relationships between the tertiles of 2-year changes in adiponectin and the changing values of cardiovascular disease risk factors are shown in Table 2. ANCOVA, adjusted for confounding factors, showed that hsCRP levels significantly decreased more over time in the highest tertile of adiponectin change than in the lowest category. By contrast, HDL levels significantly increased more over time in the highest and middle tertile of adiponectin change than in the lowest categories. Similar results were also observed in the sex-specific tertiles of adiponectin change at the 1-year follow up (data not shown). Tests for interaction between the categories of adiponectin change and other confounders in the final models were not statistically significant.

☆ Sources of funding: This study was supported by a Grant-in-Aid for "Knowledge Cluster Initiative" from the Ministry of Education, Culture, Sports, Science and Technology of Japan.
* Corresponding author at: Department of Nutrition and Food Hygiene, School of Public Health, Tianjin Medical University, 22 Qixiangtai Road, Heping District, 300070 Tianjin, People's Republic of China. Tel.: +86 22 2354 2761.
E-mail address: nkj08094@gmail.com (K. Niu).

http://dx.doi.org/10.1016/j.ijcard.2012.11.020

Table 1
Age-adjusted baseline characteristics of the participants according to tertiles of 2-year changes in adiponectin (n=980).[a]

	Sex-specific tertiles of 2-year changes in adiponectin, n (range, μg/ml)			P value[b]
	327 (male, −4.70–0.48; female, −5.50–0.07)	326 (male, 0.48–1.40; female, 0.15–1.78)	327 (male, 1.40–8.05; female, 1.78–9.30)	
Age (years)	45.5 (44.4, 46.6)[c]	46.2 (45.1, 47.3)	46.7 (45.6, 47.8)	0.32
BMI (kg/m^2)	23.5 (23.1, 23.8)	23.7 (23.4, 24.1)	22.6 (22.2, 23)[d]	0.0001
SBP (mm Hg)	126.2 (124.5, 127.9)	126.6 (124.9, 128.3)	125.3 (123.6, 127)	0.54
DBP (mm Hg)	78.7 (77.5, 79.9)	79.3 (78.1, 80.5)	77.9 (76.7, 79.1)	0.26
FBS (mg/dl)	97.2 (95.1, 99.3)	95.4 (93.3, 97.5)	94.7 (92.6, 96.7)	0.23
TG (mg/dl)	134.7 (125.4, 144.1)	126.6 (117.3, 136)	106.9 (97.5, 116.2)[d,e]	0.0001
LDL (mg/dl)	121.9 (118.5, 125.4)	122.1 (118.7, 125.5)	117.4 (114.0, 120.8)	0.10
HDL (mg/dl)	55.5 (54.0, 57.0)	53.8 (52.3, 55.4)	58.3 (56.8, 59.8)[d,e]	<0.001
hsCRP (mg/L)	0.7 (0.3, 1.1)	1.3 (0.9, 1.7)	1.2 (0.7, 1.6)	0.13
Adiponectin (μg/ml)	7.8 (7.4, 8.2)[e]	6.2 (5.8, 6.6)	8.2 (7.8, 8.6)[e]	<0.0001
Tertile of total energy intake (%)				
Middle (range: 1647.2–2095.6 kcal/d)	29.4	35.3	29.1	0.16
High (range: 2097.1–5345.6 kcal/d)	31.2	27.9	34.9	0.18
Tertile of physical activity (%)				
Middle (range: 0.55–20.0 Mets hours/week)	38.5	38.7	33.3	0.31
High (range: > 20.0 Mets hours/week)	33.6	29.1	41.3 6	<0.01
Smoker (%)				
Current smoker	43.1	50.9	42.5	0.06
Ex-smoker	11.6	11.7	13.2	0.80
Drinking status (%)				
Everyday	27.8	27.6	26.9	0.84
Sometime	45.6	50.0	52.6	0.11
Education (≥college, %)	25.4	24.9	26.3	0.90
Use of medications during the follow up				
Anti-hypertensive	13.8	14.1	13.2	0.87
Anti-diabetic	7.0	8.0	9.5	0.59
Lipid-lowering	18.7	22.1	23.2	0.46

[a] BMI, body mass index; SBP, systolic blood pressure; DBP, diastolic blood pressure; FBS, fasting blood sugar; TG, triglyceride; LDL, low density lipoprotein cholesterol; HDL, high-density lipoprotein-cholesterol; hsCRP, high-sensitivity C-reactive protein.
[b] Analysis of covariance or logistic regression analysis adjusted for age and sex where appropriate.
[c] Adjusted least squares mean (95% confidence interval) (all such values).
[d] Significantly different from the lowest tertile of change in adiponectin (Bonferroni correction): $P<0.05$.
[e] Significantly different from the middle tertile of change in adiponectin (Bonferroni correction): $P<0.05$.

This longitudinal study has shown that the longitudinal change in serum adiponectin levels is beneficially related with the changes in several CVD risk factors (HDL and hsCRP). The present results are consistent with several population-based prospective studies of apparently healthy persons, indicating that elevated adiponectin levels were related with a lower risk for CVD [7]. But, these results are not consistent with an early prospective study, which showed that a higher longitudinal increase in adiponectin predicted increased mortality in older persons [3]. The study investigated the relationship between the end levels or long-term change in adiponectin and mortality among an advanced old age population (age ≥ 65 years). The results indicated that adiponectin increased with age, and that higher end levels of adiponectin (≥20 mg/L) predicted increased all-cause mortality. Interestingly, this study also indicated an important piece of information, which is that the relation is significantly inverted in the lower portion of distribution (adiponectin levels<20 mg/L). Compared to that study, our subjects were younger, and those with an ending adiponectin level≥20 mg/L were fewer (only 9 subjects). Thus, the differences in end adiponectin levels and age groups may partly explain the conflicting results. Further study is needed to confirm this finding and whether an adiponectin level of ≥20 mg/L is a useful cutoff for an unhealthy state in different age groups.

As an explanation for this cutoff, Kizer et al. [3], discussed the possibility that very high levels, much like longitudinal increases, may predominantly signal and/or contribute to greater homeostatic dysregulation accounting for their adverse prognostic implications. Similarly, a current

Table 2
Adjusted relationships of tertiles of 2-year changes in adiponectin to the changes of cardiovascular disease risk factors during 3 year follow up.[a]

Two-years follow-up (n=980)	Sex-specific tertiles of 2-year changes in adiponectin, n (range, μg/ml)			P value[b,c]
	327 (male, −4.70–0.48; female, −5.50–0.07)	326 (male, 0.48–1.40; female, 0.15–1.78)	327 (male, 1.40–8.05; female, 1.78–9.30)	
SBP (mm Hg)	−0.91 (−2.94, 1.11)[d]	−0.52 (−2.52, 1.47)	−1.63 (−3.63, 0.36)	0.44
DBP (mm Hg)	0.5 (−1.05, 2.04)	0.95 (−0.57, 2.48)	0.25 (−1.27, 1.77)	0.56
FBS (mg/dl)	4.14 (1.6, 6.67)	2.31 (−0.18, 4.8)	2.66 (0.17, 5.15)	0.20
TG (mg/dl)	8.72 (−7.06, 24.49)	13.13 (−2.32, 28.59)	8.16 (−7.34, 23.66)	0.72
LDL (mg/dl)	−4.69 (−8.1, −1.27)	−4.38 (−7.74, −1.02)	−6.34 (−9.72, −2.96)	0.36
HDL (mg/dl)	0.12 (−1.22, 1.46)	1.89 (0.57, 3.21)[e]	2.67 (1.35, 3.99)[e]	<0.0001
hsCRP (mg/L)	0.83 (0.05, 1.6)	0.13 (−0.63, 0.89)	−0.14 (−0.91, 0.62)[e]	0.01

[a] SBP, systolic blood pressure; DBP, diastolic blood pressure; FBS, fasting blood sugar; TG, triglyceride; LDL, low density lipoprotein cholesterol; HDL, high-density lipoprotein-cholesterol; hs-CRP, high-sensitive C-reactive protein.
[b] Analysis of covariance.
[c] Adjusted for age, the interval changes of body mass index, total energy intake, and physical activity, smoking status, drinking status, educational levels, the use of anti-hypertensive, anti-diabetic, and lipid-lowering agents during the follow up, baseline value of each factor.
[d] Adjusted least squares mean (95% confidence interval) (all such values).
[e] Significantly different from the lowest tertiles of change in adiponectin (Bonferroni correction): $P<0.01$.

review also indicates adiponectin resistance as a new risk factor for CVD according to some basic studies [8]. Furthermore, higher adiponectin reduced the risk of nonfatal CVD, but increased the risk of CVD mortality, particularly in patients with prevalent CVD in a higher age group (50–75 y) [7]. In this study, the authors hypothesized that adiponectin protects against metabolic and vascular diseases, but in patients already afflicted with CVD, adiponectin is compensatively up-regulated and, therefore, indicates a high mortality risk [7].

Several other prospective studies have also indicated that higher levels of adiponectin were related with an increased risk of total and cardiovascular mortality in older persons [9,10], but have not analyzed whether having a cutoff of adiponectin results in a U-shaped relationship between adiponectin levels and adverse outcomes. Moreover, epidemiological studies have revealed that high levels of adiponectin were related with the severity of congestive heart failure [5]. However, this review also suggested that increased adiponectin production in patients with heart failure is a part of compensatory mechanisms against oxidative stress and inflammation. Increased adiponectin production might contribute, at least in part, to the metabolic and structural remodeling of the failing heart via activation of AMP-activated protein kinase and induction of cyclooxygenase-2 [5].

In summary, an increase in adiponectin with age may be caused by 2 conditions: 'pathologic' and 'physiologic' increase. The 'pathologic' increase predicted an increased risk of total and cardiovascular mortality, particularly in older populations or patients with prevalent CVD, yet 'physiologic' increase generally reflects greater fitness in an apparently healthy population. Therefore, analyzing the cause of increased adiponectin with age is an important step toward understanding the role or meaning of increased adiponectin production. For example, a cross-sectional study indicated a meaningful result which is that renal function decline is related to increases in plasma adiponectin levels in older persons (age≥65 y), but not in younger persons (age<65 y), so the decline in renal function with age may in part contribute to the age-related increase in adiponectin levels [11]. This relationship may partially explain the intricate relationship between adiponectin levels and cardiovascular mortality in older persons. More in-depth studies are needed to explore the exact mechanism and function of increased adiponectin production under different pathophysiological conditions and in different age groups.

The present study has two limitations. Firstly, because this is an observational study, we could not conclude whether increased adiponectin with age has a causal effect on the change in CVD risk factors. Secondly, since high molecular weight adiponectin, a more physiologically active form, has not been assessed, we cannot intensively analyze the relationships between these molecules and the change in CVD risk factors [12].

In conclusion, this study identified that an increase in adiponectin is beneficially related to the change in risk factors for CVD over a 3-year follow-up period. These results suggest that increased adiponectin with age may have a beneficial effect on the prevention of CVD among an apparently healthy middle-aged population.

Acknowledgments

We gratefully acknowledge all the men and women who participated in the study and Sendai Oroshisho Center for the possibility to perform the study.

Author contributions: Kaijun Niu: study concept and design, acquisition of subjects and data, analysis and interpretation of data, and preparation of manuscript.

Yoritoshi Kobayashi: acquisition of subjects and data.

Lei Guan: acquisition of subjects and data.

Haruki Monma: acquisition of subjects and data.

Hui Guo: acquisition of subjects and data.

Yufei Cui: acquisition of subjects and data.

Atsushi Otomo: acquisition of subjects and data.

Masahiko Chujo: acquisition of subjects and data.

Ryoichi Nagatomi: study concept, acquisition of subjects and data, and analysis and interpretation of data.

References

[1] Amasyali B, Kilic A, Celik T, Iyisoy A. A new frame in thromboembolic cardiovascular disease: adipocytokine. Int J Cardiol 2008;139:100–2.
[2] Kizer JR, Arnold AM, Strotmeyer ES, et al. Change in circulating adiponectin in advanced old age: determinants and impact on physical function and mortality. The Cardiovascular Health Study All Stars Study. J Gerontol A Biol Sci Med Sci 2010;65:1208–14.
[3] Kizer JR, Arnold AM, Jenny NS, et al. Longitudinal changes in adiponectin and inflammatory markers and relation to survival in the oldest old: the Cardiovascular Health Study All Stars study. J Gerontol A Biol Sci Med Sci 2011;66:1100–7.
[4] Chang LC, Huang KC, Wu YW, et al. The clinical implications of blood adiponectin in cardiometabolic disorders. J Formos Med Assoc 2009;108:353–68.
[5] Shimmura K. Is adiponectin a bystander or a mediator in heart failure? The tangled thread of a good-natured adipokine in aging and cardiovascular disease. Heart Fail Rev 2010;15:457–66.
[6] Guo H, Niu K, Monma H, et al. Association of Japanese dietary pattern with serum adiponectin concentration in Japanese adult men. Nutr Metab Cardiovasc Dis 2012;22:277–84.
[7] Dekker JM, Funahashi T, Nijpels G, et al. Prognostic value of adiponectin for cardiovascular disease and mortality. J Clin Endocrinol Metab 2008;93:1489–96.
[8] Lau WB, Tao L, Wang Y, Li R, Ma XL. Systemic adiponectin malfunction as a risk factor for cardiovascular disease. Antioxid Redox Signal 2011;15:1863–73.
[9] Wannamethee SG, Whincup PH, Lennon L, Sattar N. Circulating adiponectin levels and mortality in elderly men with and without cardiovascular disease and heart failure. Arch Intern Med 2007;167:1510–7.
[10] Poehls J, Wassel CL, Harris TB, et al. Association of adiponectin with mortality in older adults: the Health, Aging, and Body Composition Study. Diabetologia 2009;52:591–5.
[11] Isobe T, Saitoh S, Takagi S, et al. Influence of gender, age and renal function on plasma adiponectin level: the Tanno and Sobetsu study. Eur J Endocrinol 2005;153:91–8.
[12] Lara-Castro C, Luo N, Wallace P, Klein RL, Garvey WT. Adiponectin multimeric complexes and the metabolic syndrome trait cluster. Diabetes 2006;55:249–59.

Please cite this article as: Niu K, et al. Longitudinal changes in the relationship between serum adiponectin concentration and cardiovascular risk factors among apparently ... Int J Cardiol (2012), http://dx.doi.org/10.1016/j.ijcard.2012.11.020

Artificial Organs

Communication

Medical Responses Following the Sendai Quake (East Japan Earthquake, March 11, 2011)

*Tomoyuki Yambe, †Muneichi Shibata, †Taketada Sumiyoshi, †Yoshiaki Mibiki, †Noboru Osawa, ‡Yoshiaki Katahira, ‡Minoru Yambe, ‡Kou-ichi Tabayashi, §Masanori Yamashina, §Eiji Sato, §Shinichi Sato, §Tetsuo Yagi, ¶Makoto Watanabe, ¶Yoshihira Akinno, **Masanori Munakata, ††Naoki Owada, *Masatoshi Akiyama, *Yoshikatsu Saiki, *Norihiro Sugita, and *Makoto Yoshizawa

*Tohoku University, Sendai; †Miyagi Cardiovascular Respiratory Center, Miyagi; ‡Tohoku Kouseinenkin Hospital, Sendai; §Sendai City Hospital, Sendai; ¶Miyagi Shakaihoken Hospital, Sendai; **Tohoku Rosai Hospital, Sendai; and ††Miyagi Cancer Center, Natori, Japan

On March 11, 2011, disaster struck the east coast of Japan (1–7) named of the Great East Japan Earthquake or Sendai Quake (8) (Wikipedia).

Japan had been expecting a large earthquake for a long time. The Sendai Quake involved three epicenters at various distances out to sea. The force of the magnitude 9.0 quake caused an enormous tsunami that deluged the cities on the eastern seashore in the Tohoku area (northeast coast of Japan). In Minamisanriku City, for example, almost all buildings were lost after the earthquake and tsunami struck (Fig. 1).

To add to the disaster, fires broke out after the earthquake and tsunami. Large portions of the cities near the eastern seashore were completely lost. In addition to these disasters, a meltdown occurred at the Fukushima nuclear power plant. Radioactive contamination occurred not only throughout Japan but also all over the world.

Unfortunately, detailed medical data about the aftermath of the Sendai Quake are not available because all medical records were lost with the hospital buildings, especially in the tsunami areas near the eastern seashore. Detailed information of the number of dead has not yet been summarized, even by the Japanese government. As many as 20 000 people have been reported lost as a result of this complex emergency. The medical response following the earthquake and tsunami in eastern Japan has not been clearly described. This short report is intended to provide details of this response.

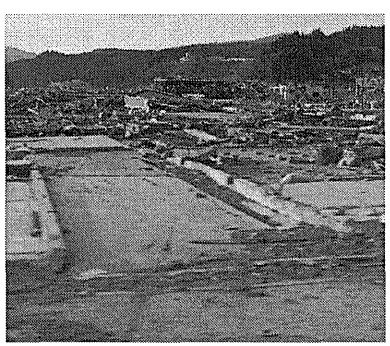

FIG. 1. Minamisanriku City after the tsunami (photo by the Miyagi Medical Support team).

doi:10.1111/j.1525-1594.2012.01522.x

Received January 2012; revised May 2012.

Address correspondence and reprint requests to Dr. Tomoyuki Yambe, Department of Medical Engineering and Cardiology, Tohoku University, 4-1 Seiryo-machi, Aoba-ku, Sendai 980-8575, Japan. E-mail: yambe@idac.tohoku.ac.jp

Presented in part at the 19th Congress of the International Society for Rotary Blood Pumps, held on September 8–10, 2011, in Louisville, KY, USA.

MEDICAL RESPONSE TO THE SENDAI QUAKE

The Tohoku University Hospital is located in Sendai City in the area that sustained the most damage from the tsunami and earthquake. Despite the sadness that flooded the nation after the disaster, one consolation was that no fatalities occurred among patients, doctors, nurses, or other staff at the University Hospital. The response to the disaster at this hospital can be examined in four stages.

The first stage involved initial recovery and preparation for dealing with the aftereffects of the disaster. First, the safety of all patients and staff members was secured. Then, medical resources were mobilized according to the hospital's triage tag system. Everything in the University Hospital was rearranged to accommodate disaster victims. All routine surgeries and medical examinations were postponed, and the outpatient clinic was closed. When disaster victims arrived at the University Hospital, they received green, yellow, red, or black tags, according to the methodology of the triage tag system. Patients with green tags were treated in the outpatient clinic, those with yellow tags went to the intensive care unit, those with red tags went to the operating room, and those with black tags went to the building of basic science. Appropriate treatment was delivered in these various locations.

In the second stage, normal hospital functions were restored. Planning began for the acceptance of patients being transferred from damaged hospitals on the eastern coast. Shortages of all medical resources had been anticipated, so messages were sent to all university hospitals in Japan to gather drugs and food and to prepare disaster medical assistance teams.

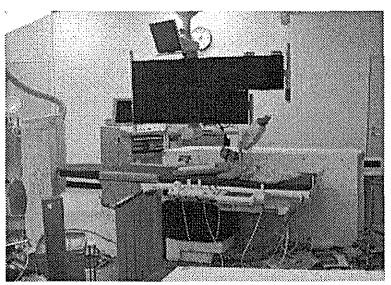

FIG. 2. Cardiac catheterization room after the Sendai Quake.

FIG. 3. Shelter after the tsunami (photo by Miyagi Medical Support Team).

In the third stage, teams of doctors and nurses, along with medical resources, food, and drugs, were sent to the afflicted hospitals. Thousands of medical support teams were sent to the cities on the eastern coast affected by the tsunami. The fourth stage, which involves reconstruction of medical support buildings in the damaged area, is still ongoing.

THE STATE OF MEDICAL CARE AFTER THE TSUNAMI

Challenges were many throughout the region. Creative solutions to various problems had to be sought. For example, in the Miyagi Cardiovascular Respiratory Center, electric power and water supplies were down. Patients in stable condition were therefore discharged, and emergency patients were treated using equipment powered by in-house power generation units.

Despite all the efforts to meet people's needs, medical resources were inadequate because of the magnitude of the disaster. Medical equipment was damaged and debris was everywhere (Fig. 2). Medical teams visited shelters after the tsunami (Fig. 3). The Miyagi Medical Support team diagnosed and treated in a temporary shelter.

An emergency care unit is present at Sendai City Hospital. Although ambulances had been salvaged from the disaster area, destroyed roads and traffic jams prevented them from transporting patients to the hospital. Many patients came to Tohoku Rosai Hospital, located in the city center, on foot. The

volume of patients was large, and the hospital was so busy that medical staff were unable to return to their homes.

Miyagi Shakaihoken Hospital is located near the coast. Many tsunami victims went to that hospital, but the surgery department's systems were down. Patients could not be adequately treated without functional operating rooms.

Some of the most severe damage was observed at Kesennuma City near the seashore. All buildings in that area were destroyed by the earthquake, tsunami, and fire; therefore, people were required to go to refuge centers. Control of hypertension, diabetes, and many other health disorders was difficult in these makeshift conditions, and newly developed electronic doctor's bags were used to control these conditions.

Furthermore, the Sendai Airport was also completely destroyed by the tsunami, but it was restored soon after by the TOMODACHI operation carried out by the US Army.

FUKUSHIMA NUCLEAR POWER PLANT MELTDOWN

The Fukushima nuclear power plant accident exacerbated the already difficult situation in hospitals. On March 11, a meltdown at the power plant was reported, and hydrogen explosions followed on March 12 and 14. Radioactive materials were scattered as a result of these accidents. The plant was shut down.

In Japan, discussion is ongoing concerning the future consequences of the radiation leaks resulting from the accident at Fukushima (9–12). In the early 1960s, Japan experienced a large amount of strontium, cesium, and plutonium fallout caused by atomic bomb experiments conducted by several countries, including the USA, France, the Soviet Union, and China. Plutonium levels in Japan were estimated to be 100 000 times higher in the 1960s compared with recent levels. But the life span of Japanese people is the longest in advanced countries. No one can show the risk of radiation fallout in early 1960s. No increase in cancer incidence was observed in Japan in the early 1960s. Thus, the true risk of radiation fallout is also unclear, because double-blind tests of radiation poisoning cannot be performed.

Sendai City is located north of Fukushima. All roads from Tokyo (south of Fukushima) and other areas of Japan had been blocked between Fukushima and Tokyo, because antinuclear power activists announced a non-scientific propaganda concerning the risk of radiation material fallout. Relief supplies could not be transported into the Fukushima area because of demonstrations by the antinuclear activists. So, the relief goods could not go north to Sendai. Many patients did not survive due to a shortage of drugs and food caused by the propaganda of the antinuclear activists.

USE OF ARTIFICIAL ORGANS DURING THE DISASTER

At the time of the disaster, more than 50 patients were on respirators, whereas 11 were dependent on hemodialysis (HD) at Tohoku University Hospital. Emergency power units ensured the safety of these patients. However, all coastal hospitals had sustained devastating damage. Therefore, all patients who were dependent on HD were transported to Tohoku University Hospital. Medical resources were inadequate to meet their needs, and helicopters transferred these HD patients to other hospitals. Around 100 HD patients were transferred to the other hospitals. In particular, large numbers of HD patients were transferred to Hokkaido.

Three patients required the Nipro ventricular assistance system (VAS) support at Tohoku University Hospital during the Sendai Quake. Because emergency power started smoothly, no disruption of VAS treatment occurred.

However, certain lifelines, such as electric power, water, and gas supplies, had all been shut down in Sendai City. Therefore, patients requiring rotary blood pumps were transported to the ambulance center and subsequently moved to the University Hospital after the roads became passable. Pneumatic VAS remained useful during the disaster, which was surprising because they were situated in the hospital with the emergency power unit.

Patient care had to be performed, although medical resources were limited. For VAS and HD, the prothrombin time and international normalized ratio must be measured. These parameters had to be checked in shelters. For example, the Miyagi Medical Support Team, who visited various shelters, brought electronic medical equipment. This equipment was a lifeline for patients taking refuge in shelters, especially for those requiring life support using artificial organs.

TELEMEDICINE USING THE ELECTRONIC DOCTOR'S BAG

Medical resources were inadequate to respond to the disaster. Medical treatment was limited because all lifelines had been compromised. Doctors and nurses took it upon themselves to visit people in shelters, travelling destroyed roads on foot to do so.

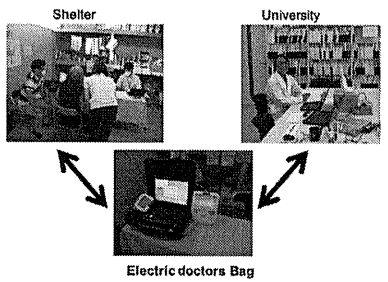

FIG. 4. Above: Clinical application of the electronic doctor's bag in a shelter in Kesennuma City. Below: The bag being tested at Tohoku University.

The electronic doctor's bag, which was invented at Tohoku University, was useful in responding to victims' needs in these emergency conditions (Fig. 4).

The electronic doctor's bag was first used in the shelter in Kesennuma City, one of the most severely damaged areas, after approval from the ethics committee of Tohoku University Graduate School of Medicine. Use of the electronic doctor's bag facilitated evaluation of the condition of patients at the shelter by doctors located at the University. At the time of the disaster, the personnel shortage precluded on-site evaluation. Therefore, telemedicine and remote medicine were thought to be useful. The electronic doctor's bag enabled electrocardiography, blood pressure measurement, and ultrasonic diagnosis to be performed at the disaster shelters. Using this newly developed system, medical personnel in the shelters were also able to confer with doctors at Tohoku University via Skype. Using this device, control of anticoagulation, blood sugar levels, and blood pressure are able to be achieved, thereby preventing adverse cardiovascular events from occurring.

SUMMARY

After the Sendai Quake, all medical resources were mobilized to respond to the disaster. However, shortages of everything caused seemingly insurmountable problems, especially in areas affected by the tsunami. Maintenance of lifelines was vital to patients requiring artificial organs.

Medical equipment preparation and planning are now under way to enable adequate response to future large disasters. Discussion is ongoing about the continued risk of radiation after the Fukushima nuclear power plant meltdown. In previous reports, no risk of increased cancer due to exposure to radiation <100 mSv was reported. In Japan, all radioactive fallout in every area has been reported daily on the governmental website since the disaster. Information about radiation levels is publicly available in Japan.

In conclusion, a detailed statistical analysis of the disaster is now under way, the results of which will be reported in the near future. The most important thing during times of disaster is the rapid recovery of lifelines.

Acknowledgments: The authors express their thanks to the disaster medical assistance teams from all over Japan and the world that provided aid to people in the Tohoku area, and to all hospitals that received and treated the hemodialysis patients. Thanks also to those who participated in the TOMODACHI operation initiated by the US Army for their efforts in restoring the Sendai Airport to operative status and aiding the people of Japan in recovering from the events of March 2011.

REFERENCES

1. Satomi S. The Great East Japan Earthquake: Tohoku University Hospital's efforts and lessons learned. *Surg Today* 2011;41:1171–81.
2. Fuse A, Igarashi Y, Tanaka T, et al. Onsite medical rounds and fact-finding activities conducted by Nippon Medical School in Miyagi prefecture after the Great East Japan Earthquake 2011. *J Nihon Med Sch* 2011;78:401–4.
3. Satoh M, Kikuya M, Ohkubo T, Imai Y. Acute and subacute effects of the great East Japan earthquake on home blood pressure values. *Hypertension* 2011;58:e193–4.
4. Tsuji M, Kanda H, Kakamu T, et al. An assessment of radiation doses at an educational institution 57.8 km away from the Fukushima Daiichi nuclear power plant 1 month after the nuclear accident. *Environ Health Prev Med* 2012;17:124–30.
5. Kanamori H, Kunishima H, Tokuda K, Kaku M. Infection control campaign at evacuation centers in Miyagi prefecture after the Great East Japan Earthquake. *Infect Control Hosp Epidemiol* 2011;32:824–6.
6. Sato M, Ishikawa T, Ujihara N, et al. Displacement above the hypocenter. *Science* 2011;332:1395.
7. Takeda M. Mental health care and East Japan Great Earthquake. *Psychiatry Clin Neurosci* 2011;65:207–12 .
8. Johnston GT. Into the next stage: Sendai quake, tsunami, test Japan's spirit. (First published in The Rafu Shimpo on March 17, 2011.) Available at: http://rafu.com/news/2011/03/itns-3/. Accessed July 18, 2012.
9. Reizenstein P. Carcinogenicity of radiation doses caused by the Chernobyl fall-out in Sweden, and prevention of possible tumors. *Med Oncol Tumor Pharmacother* 1987;4:1–5.
10. Hossono G. Ministry of Environment, 2012. Available at: http://housyasen.taiki.go.jp/. Accessed July 18, 2012.
11. Coggle JE, Lambert BE, Moores SR. Radiation effects in the lung. *Environ Health Perspect* 1986;70:261–91.
12. Zeighami EA, Morris MD. Thyroid cancer risk in the population around the Nevada Test Site. *Health Phys* 1986;50:19–32.

Toxins **2012**, *4*, 1309-1322; doi:10.3390/toxins4111309

OPEN ACCESS

toxins

ISSN 2072-6651

www.mdpi.com/journal/toxins

Article

A Metabolomic Approach to Clarifying the Effect of AST-120 on 5/6 Nephrectomized Rats by Capillary Electrophoresis with Mass Spectrometry (CE-MS)

Yasutoshi Akiyama [1,2], Yoichi Takeuchi [2,3], Koichi Kikuchi [2], Eikan Mishima [2], Yasuaki Yamamoto [2], Chitose Suzuki [2], Takafumi Toyohara [2], Takehiro Suzuki [2], Atsushi Hozawa [4], Sadayoshi Ito [2], Tomoyoshi Soga [5] and Takaaki Abe [2,3,6,*]

1 Department of Community Health Promotion, Tohoku University Graduate School of Medicine, Sendai 980-8574, Japan; E-Mail: y-akiyama@med.tohoku.ac.jp

2 Division of Nephrology, Endocrinology and Vascular Medicine, Tohoku University Graduate School of Medicine, Sendai 980-8574, Japan; E-Mails: muu-tko@med.tohoku.ac.jp (Y.T.); koichikikuchithk@yahoo.co.jp (K.K.); eikan@med.tohoku.ac.jp (E.M.); drow_rorrim@yahoo.co.jp (Y.Y.); chitose@med.tohoku.ac.jp (C.S.); toyohara@med.tohoku.ac.jp (T.T.); suzuki2i@med.tohoku.ac.jp (T.S.); db554@med.tohoku.ac.jp (S.I.)

3 Department of Clinical Biology and Hormonal Regulation, Tohoku University Graduate School of Medicine, Sendai 980-8574, Japan

4 Department of Preventive Medicine and Epidemiology, Tohoku Medical Megabank Organization, Tohoku University, Sendai 980-8573, Japan; E-Mail: hozawa-thk@umin.ac.jp

5 Institute for Advanced Biosciences, Keio University, Tsuruoka, Yamagata 997-0052, Japan; E-Mail: soga@sfc.keio.ac.jp

6 Division of Medical Science, Tohoku University Graduate School of Biomedical Engineering, Sendai 980-8574, Japan

* Author to whom correspondence should be addressed; E-Mail: takaabe@med.tohoku.ac.jp; Tel.: +81-22-717-7163; Fax: +81-22-717-7168.

Received: 18 July 2012; in revised form: 19 September 2012 / Accepted: 26 October 2012 / Published: 14 November 2012

Abstract: The oral adsorbent AST-120 is composed of spherical carbon particles and has an adsorption ability for certain small-molecular-weight compounds that accumulate in patients with chronic kidney disease (CKD). So far, very few compounds are known to be adsorbed by AST-120 *in vivo*. To examine the effect of AST-120 *in vivo*, we comprehensively evaluated the plasma concentrations of 146 compounds (61 anions and 85 cations) in CKD model rats, with or without four weeks of treatment with AST-120. By capillary electrophoresis with mass spectrometry, we identified 6 anions and 17 cations that were significantly decreased by AST-120 treatment. In contrast, we also identified 2 cations that were significantly increased by AST-120. Among them, 4 anions, apart from indoxyl sulfate and hippurate, and 19 cations were newly identified in this study. The plasma levels of *N*-acetyl-neuraminate, 4-pyridoxate, 4-oxopentanoate, glycine, γ-guanidinobutyrate, *N*-γ-ethylglutamine, allantoin, cytosine, 5-methylcytosine and imidazole-4-acetate were significantly increased in the CKD model compared with the sham-operated group, and were significantly decreased by AST-120 treatment. Therefore, these 10 compounds could be added as uremic compounds that indicate the effect of AST-120 treatment. This study provides useful information not only for identifying the indicators of AST-120, but also for clarifying changes in the metabolic profile by AST-120 treatment in the clinical setting.

Keywords: AST-120; uremic toxin; CE-MS

1. Introduction

Chronic kidney disease (CKD) is a global health problem that carries a substantial risk for cardiovascular morbidity and death [1,2]. With the progression of CKD, various uremic toxins accumulate, subsequently causing renal damage and hypertension [3–5]. Because most uremic toxins are excreted into the urine, once uremic toxins accumulate in CKD patients, eliminating them is very difficult because of reduced renal function. So far, the only established therapy to eliminate uremic toxins in CKD patients is AST-120 [6,7]. AST-120 is an oral adsorbent that consists of spherical carbon particles and adsorbs uremic toxins and/or their precursors in the intestines. It is reported that AST-120 inhibits the progression of not only CKD but also cardiovascular diseases [6]. One of the best-known uremic toxins whose plasma level is decreased by AST-120 treatment is indoxyl sulfate [8]. AST-120 decreases the plasma level of indoxyl sulfate by adsorbing the precursor of indoxyl sulfate, *i.e.*, the indole, resulting in the reduction of indoxyl sulfate production in the liver. In addition to indoxyl sulfate, some compounds whose plasma levels are decreased by AST-120 treatment have been reported, such as hippurate, phenyl sulfate, 4-ethylphenyl sulfate, p-cresyl sulfate [9] and advanced glycation end products [10]. However, the target compounds of AST-120 have not been fully elucidated.

To clarify the compounds whose plasma concentrations are changed by AST-120 treatment, we comprehensively quantified and analyzed the plasma levels of over 500 compounds in 5/6 nephrectomized (5/6Nx) rats with or without AST-120 treatment using capillary electrophoresis with mass spectrometry (CE-MS).

2. Materials and Methods

2.1. Materials

Oral adsorbent AST-120 (Kremezin®) was kindly provided by Kureha Corporation (Tokyo, Japan).

2.2. Animals and Treatment

Wistar rats were obtained from Charles River (Kanagawa, Japan). At the age of nine weeks, 5/6 nephrectomy or sham operation was performed as previously reported [11]. Ten weeks after the operation, systolic blood pressure (SBP), body weight (BW), plasma creatinine (Cr) and creatinine clearance (Ccr) were measured, and then 5/6Nx rats were randomized into two groups, a control group (n = 13) and the AST-120 group (n = 12). The AST-120 group was fed powder chow (CE-2, CLEA Japan, Inc., Tokyo, Japan) containing 8% (w/w) AST-120 for four weeks, whereas the sham-operated (n = 3) and control (n = 13) groups were fed powder chow alone. After four weeks of treatment, SBP, BW, Cr and Ccr were measured again, the rats were then sacrificed and the plasma was subjected to CE-MS analysis. This animal experiment was approved by the Center for Laboratory Animal Research, Tohoku University.

2.3. Blood Pressure and Biochemical Measurement

Systolic blood pressure was measured by the tail cuff method (MK-2000, Muromachi Kikai, Tokyo, Japan) in a conscious state. Plasma creatinine was measured with iSTAT (Abbott Point of Care Inc., Princeton, NJ). Urinary creatinine was enzymatically measured (SRL Inc., Tokyo, Japan).

2.4. CE-MS Measurement for Metabolome Analysis

A comprehensive and quantitative analysis of charged metabolites by CE-MS was performed [12–14]. Plasma (50 μL) was immediately plunged into methanol (450 μL) containing internal standards (20 μM each of methionine sulfone (Wako, Osaka Japan) for cations, MES (Dojindo, Kumamoto, Japan) and CSA (D-Camphol-10-sulfonic acid, Wako). Then, de-ionized water (200 μL) and chloroform (500 μL) were added, and the mixture was thoroughly mixed. The solution was centrifuged at 4600× g for 5 min at 4 °C, and the upper aqueous layer was centrifugally filtered through a Millipore 5000 Da cutoff filter (Millipore, Billerica, MA) to remove proteins. The filtrate was lyophilized and dissolved in 25 μL of Milli-Q water containing reference compounds (200 μM each of 3-aminopyrrolidine (Sigma Aldrich, St. Louis, MO) and trimesate (Wako) prior to capillary electrophoresis with electrospray ionization time-of-flight mass spectrometry (CE-TOFMS) analysis. All CE-TOFMS experiments were performed using the Agilent CE capillary electrophoresis system (Agilent Technologies, Waldbronn, Germany), the Agilent G3250AA LC/MSD TOF system (Agilent Technologies, Palo Alto, CA), the Agilent 1100 series binary HPLC pump, the G1603A Agilent CE-MS adapter, and the G1607A Agilent CE-ESI-MS sprayer kit. For data acquisition, we used G2201AA Agilent ChemStation software for CE and the Analyst QS for Agilent TOFMS software [14].

Cationic metabolites were separated in a fused silica capillary (50 μm i.d. × 100 cm) filled with 1 M formic acid as the electrolyte [15]. A sample solution was injected at 50 mbar for 3 s (3 nL) and 30 kV of voltage was applied. The capillary temperature and the sample tray were set at 20 °C and below 5 °C, respectively. Methanol water (50% v/v) containing 0.1 μM Hexakis (2,2-difluorothoxy) phosphazene was delivered as the sheath liquid at 10 μL/min. ESI-TOFMS was operated in the positive ion mode, and the capillary voltage was set at 4 kV. A flow rate of heated dry nitrogen gas (heater temperature 300 °C) was maintained at 10 psig. In TOFMS, the fragmentor, skimmer and Oct RFV voltages were set at 75, 50, and 125 V, respectively. Automatic recalibration of each acquired spectrum was performed using reference masses of reference standards; ([^{13}C isotopic ion of protonated methanol dimer (2MeOH + H)]$^+$, m/z 66.0632) and ([Hexakis (2,2-difluorothoxy)phosphazene + H]$^+$, m/z 622.0290). Exact mass data were acquired at a rate of 1.5 spectra/s over a 50–1000 m/z range.

As the reference [16], anionic metabolites were separated in a COSMO(+), chemically coated with a cationic polymer, capillary (50 μm i.d. × 100 cm) (Nacalai Tesque, Kyoto, Japan) filled with 50 mM ammonium acetate solution (pH 8.5) as the electrolyte [17]. A sample solution was injected at 50 mbar for 30 s (30 nL) and −30 kV of voltage was applied. A platinum electrospray ionization spray needle was replaced with the original Agilent stainless steel needle [16]. A 5 mM ammonium acetate in 50% (v/v) methanol-water containing 0.1 μM Hexakis (2,2-difluorothoxy) phosphazene was delivered as the sheath liquid at 10 μL/min. ESI-TOFMS was operated in the negative ion mode, and the capillary voltage was set at 3.5 kV. In TOFMS, the fragmentor, skimmer and Oct RFV voltages were set at 100, 50, and 200 V, respectively. Automatic recalibration of each acquired spectrum was performed using reference masses of reference standards; ([^{13}C isotopic ion of deprotonated acetic acid dimer ($2CH_3COOH$-H)]$^-$, m/z120.0384) and ([Hexakis(2,2-difluorothoxy)phosphazene + deprotonated acetic acid(CH_3COOH-H)]$^-$, m/z 680.0355). Other conditions were as the same as in cationic metabolite analysis.

2.5. Statistics

The data were expressed as means ± SD. Samples below the detection limit were assigned the value of the detection limit and subjected to statistical analysis. However, compounds whose levels were below the detection limit in all samples were excluded for this analysis.

Analysis of variance (ANOVA) was performed with the Benjamini-Hochberg multiple testing correction for the false discovery rate at 0.05. Tukey's procedure for multiple comparisons was applied as post hoc test. $P < 0.05$ was considered to be significant.

3. Results

3.1. Biological Profiles and CE-MS Analysis

There were no significant differences in the total amounts of food intake (data not shown), SBP, BW, Cr and Ccr between the control and AST-120 groups throughout the experiment (Table 1). An AST-120 rat died of uremia at three weeks. SBP and Cr were significantly lower and Ccr was significantly higher in the sham-operated group than in both the control and AST-120 groups at four weeks of treatment.

Using CE-MS analysis, 220 anionic and 300 cationic compounds whose molecular weights ranged from 71.1 to 784.2 m/z were analyzed and quantified. Among them, 146 compounds (61 anions and 85 cations) were detected (Supplementary Tables S1 and S2). The other compounds (159 anions and 215 cations) were below the detection limit in all samples and were excluded for the analysis.

Table 1. Parameters before and four weeks after administration of AST-120 to chronic kidney disease (CKD) rats. ** $p < 0.01$ *vs.* control at four weeks.

	Sham (n = 3)	Control (n = 13)		AST-120 (n = 11)	
	4 weeks	0 week	4 weeks	0 week	4 weeks
BW (g)	493 ± 15	452 ± 22	490 ± 19	462 ± 17	486 ± 43
SBP (mmHg)	124 ± 7 **	173 ± 20	177 ± 21	169 ± 23	169 ± 24
Cr (mg/dL)	0.60 ± 0.10 **	1.03 ± 0.12	1.06 ± 0.26	1.04 ± 0.18	0.98 ± 0.26
Ccr (mL/min)	2.09 ± 0.29 **	1.06 ± 0.26	1.29 ± 0.38	1.11 ± 0.28	1.43 ± 0.4

3.2. Anions

As shown in Figures 1 and 2, the plasma concentrations of six anionic compounds, 4-oxopentanoate, hippurate, *N*-acetylneuraminate, 4-pyridoxate, indoxyl sulfate and o-hydroxybenzoate, were significantly decreased in the AST-120 group compared to those of the control (A + B group in Figure 1). Four compounds, 4-oxopentanoate, *N*-acetylneuraminate, 4-pyridoxate and o-hydroxybenzoate, were newly indentified as compounds that were significantly decreased by AST-120 treatment. The plasma levels of 4-oxopentanoate, hippurate, N-acetylneuraminate and 4-pyridoxate were significantly increased in the control compared with the sham-operated group and significantly decreased by the AST-120 treatment (B group in Figure 1).

Figure 1. Venn diagram of 61 anionic and 85 cationic compounds evaluated in this study. (**A**) indoxyl sulfate and o-hydroxybezoate. (**B**) 4-oxopentanoate, hippurate, *N*-acetylneuraminate and 4-pyridoxate. (**C**) anthranilate, glycerophosphorylcholine, nicotinamide, glutamine, asparagine, dihydrouracil, glutamate, creatine, γ-butyrobetaine and 1-methylnicotinamide. (**D**) glycine, γ-guanidinobutyrate, *N*-γ-ethylglutamine, allantoin, cytosine, 5-methylcytosine and imidazole-4-acetate. (**E**) Trimethylamine *N*-oxide. (**F**) Tryptophan. Groups B and D may represent uremic compounds that indicate the effects of AST-120.

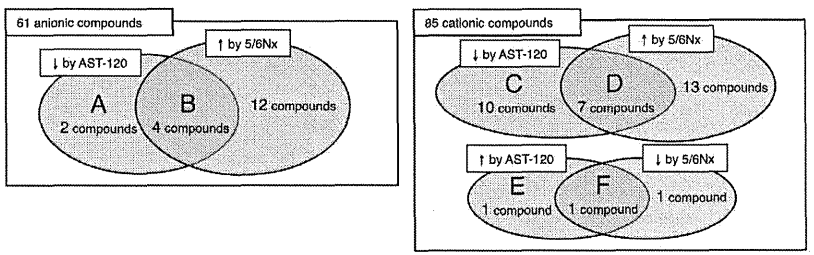

Figure 2. The six anionic compounds that were significantly decreased by AST-120 treatment compared to control.

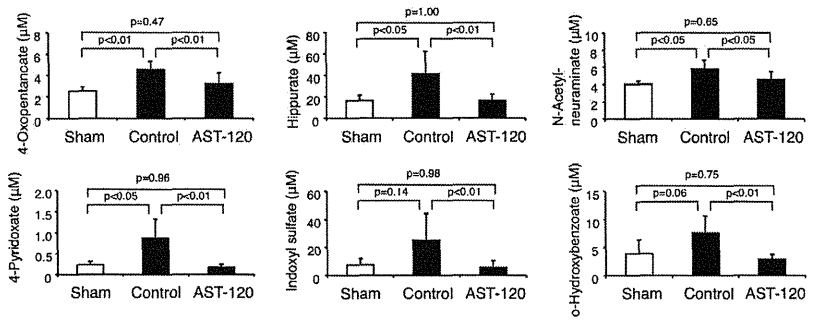

3.3. Cations

As shown in Figures 1 and 3A, the plasma concentrations of 17 cationic compounds, glycine, γ-guanidinobutyrate, *N*-γ-ethylglutamine, allantoin, cytosine, 5-methylcytosine, imidazole-4-acetate, anthranilate, glycerophosphorylcholine, nicotinamide, glutamine, asparagine, dihydrouracil, glutamate, creatine, γ-butyrobetaine and 1-methylnicotinamide, were significantly decreased in the AST-120 group compared with those in the control (C + D group in Figure 1). All of them are newly identified as compounds that were significantly decreased by AST-120 treatment. The plasma levels of glycine, γ-guanidinobutyrate, *N*-γ-ethylglutamine, allantoin, cytosine, 5-methylcytosine and imidazole-4-acetate were significantly increased in the control group compared with the sham-operated group and significantly decreased by AST-120 treatment (D group in Figure 1).

On the other hand, as shown in Figure 3B, the plasma concentrations of tryptophan and trimethylamine *N*-oxide were significantly increased in the AST-120 group compared to those in the control group (E + F group in Figure 1). Both of them are newly identified as compounds that were significantly increased by AST-120 treatment. The plasma tryptophan concentration was significantly decreased by 5/6Nx and increased to the level of the sham-operated group by AST-120 treatment (F group in Figure 1).

Figure 3. The 19 cationic compounds that were significantly decreased or increased by AST-120 treatment compared to control. (**A**) Compounds that were significantly decreased by AST-120. (**B**) Compounds that were significantly increased by AST-120.

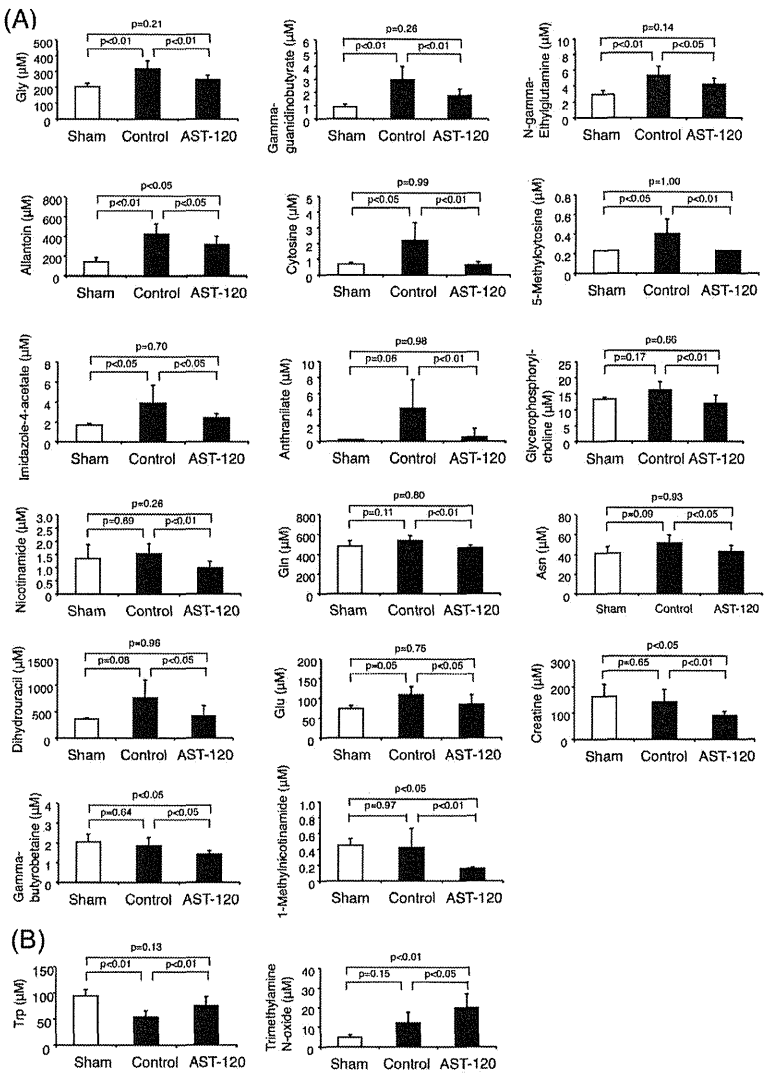

4. Discussion

In this study, using the CE-MS method [11–14,18], we comprehensively analyzed over 500 compounds and quantified 146 compounds (Supplementary Tables S1 and S2). We identified 25 compounds (6 anions and 19 cations) whose plasma concentrations were significantly changed by AST-120 treatment in 5/6Nx rats (the results are summarized in Figure 1 and Table 2). Among them, the plasma levels of 11 compounds were significantly increased in the 5/6Nx rats compared with the sham-operated rats, suggesting that they were uremic compounds whose plasma concentrations were significantly decreased by AST-120 treatment (B and D groups in Figure 1). It has been reported that 4-oxopentanoate, hippurate, allantoin and cytosine also accumulate in CKD patients [13,19,20], suggesting that these four compounds may be common uremic compounds for both rats and human. On the other hand, among the compounds whose plasma concentrations were not changed by 5/6 nephrectomy in this experiment, some have been reported to be accumulated in 5/6Nx rats or CKD patients (Table 2). For example, although it is well known that indoxyl sulfate accumulates in both 5/6Nx rats and CKD patients [8,19], there was no significant difference in the plasma indoxyl sulfate concentration between the sham-operated and control groups in this study. Probably, this was because of the small number ($n = 3$) of sham-operated rats. Other than indoxyl sulfate, asparagine, creatine and γ-butyrobetaine have been reported to be accumulated in CKD patients [13,19]. Therefore, these compounds might be included among the uremic compounds that are indicators of the effects of AST-120. On the other hand, *N*-acetylneuraminate, 4-pyridoxate, *N*-γ-ethylglutamine, 5-methylcytosine and imidazole-4-acetate were not detected in CKD patients in our previous study [13]. Therefore, they may not be uremic compounds in humans. In addition to these, o-hydroxybenzoate, anthranilate, nicotinamide and dihydrouracil were not detected in CKD patients. These discrepancies between 5/6Nx rats and CKD patients may reflect differences in their metabolic profiles. Further studies are needed to clarify the differences in the uremic compounds and the effect of AST-120 between rats and human.

The plasma levels of creatine, γ-butyrobetaine and 1-methylnicotinamide were significantly lower in the AST-120 group than in the sham-operated group, which suggests that AST-120 may cause a shortage of these compounds. Among them, 1-methylnicotinamide is known as the major metabolite of nicotinamide. Because the plasma level of nicotinamide was also decreased by AST-120, the decrease of 1-methylnicotinamide may be caused by the decrease of nicotinamide. It has been reported that 1-methylnicotinamide and nicotinamide exert anti-inflammatory effects *in vivo* [21], and it has been also reported that 1-methylnicotinamide has anti-thrombotic activity [22] and anti-diabetic effects [23]. Therefore, the decreases of both compounds may have a bad influence on the immune system, cardiovascular system or glucose metabolism in rats. However, nicotinamide was not detected in human serum in our previous study [13]. This may be a result of differences in the profile of nicotinamide metabolism or distribution in the body between rats and human. Further studies are needed to clarify the effect of AST-120 on such compounds in human.

Although AST-120 is an adsorbent, it is unknown whether these compounds are directly adsorbed by AST-120. It is well known that the plasma indoxyl sulfate concentration is decreased by AST-120 treatment because, not indoxyl sulfate itself, but its precursor indole is adsorbed by AST-120 in the intestines. Plasma hippurate concentration is also decreased by AST-120 through adsorbing its

precursor benzoic acid [9]. By the same mechanism as indoxyl sulfate and hippurate, the plasma concentration of one metabolite can be decreased if AST-120 adsorbs its precursor and prevents it from being absorbed into the body. In addition, theoretically, compounds that undergo enterohepatic circulation could be adsorbed directly by AST-120. However, so far, little is known about the metabolism and dynamics of the compounds identified in our present study. Therefore the mechanism(s) by which plasma levels of these compounds were lowered by AST-120 still remains largely unknown.

On the other hand, the plasma levels of tryptophan and trimethylamine N-oxide were increased by AST-120 treatment. These increases cannot be explained by the adsorbing effect of AST-120. It has been reported that the plasma tryptophan level is decreased in CKD patients and 5/6Nx rats [13,24]. Because Cr and Ccr did not differ between the control and AST-120 groups, it is suggested that AST-120 recovered the decline of the plasma tryptophan level in the CKD model by unknown mechanism(s) unrelated to renal function. In contrast to tryptophan, it has previously been reported that trimethylamine *N*-oxide accumulates in CKD patients [25]. AST-120 further increased the plasma level of trimethylamine *N*-oxide in 5/6Nx rats. Recently it has been reported that trimethylamine *N*-oxide is formed from dietary phosphatidylcholine through gut-flora-dependent metabolism and promotes atherosclerosis [26]. Therefore the increased level of trimethylamine *N*-oxide may be an adverse effect of AST-120 treatment. In addition, AST-120 may have change the gut-flora composition by its adsorption mechanism in 5/6Nx rats. Further study is needed to clarify the effect of AST-120 on plasma trimethylamine N-oxide level in CKD patients.

Previously, Kikuchi *et al.* reported that indoxyl sulfate, hippurate, phenyl sulfate, 4-ethylphenyl sulfate and *p*-cresyl sulfate were identified as the indicators of the effect of AST-120 in 5/6Nx rats by liquid chromatography/tandem mass spectrometry [9]. Although there were differences in the administration period (three days in Kikuchi *et al.*'s and four weeks in ours), our experimental model was similar to that of Kikuchi *et al.* As same as the result of Kikuchi *et al.*, we also identified indoxyl sulfate and hippurate as the indicators of the effect of AST-120. However, the other compounds, *i.e.*, phenyl sulfate, 4-ethylphenyl sulfate and *p*-cresyl sulfate, were not included in the measurement list in our CE-MS method. Therefore, it is unknown whether the same results were obtained for these compounds in our experimental model. The results of Kikuchi *et al.*, and ours were summarized in Table 2.

Table 2. Changes in plasma concentration of the identified compounds in 5/6Nx rats or CKD patients. N.S. indicates that the compound concentration was not significantly changed in renal failure rats or human. Not Detected indicates that the compound concentration in plasma was lower than the detection limit of CE-MS. NA indicates that the compound was not assessed in this experiment.

Anionic compounds	In this experiment	Reported by Kikuchi *et al.* [9]	Reported in human by Toyohara T. *et al.* [13]	Others	References
4-Oxopentanoate	↑ by 5/6Nx, ↓ by AST-120		↑ in CKD patients		
Hippurate	↑ by 5/6Nx, ↓ by AST-120	↑ by 5/6Nx, ↓ by AST-120	↑ in CKD patients	↑ in uremia	[19]
N-Acetylneuraminate	↑ by 5/6Nx, ↓ by AST-120		Not Detected		
4-Pyridoxate	↑ by 5/6Nx, ↓ by AST-120		Not Detected		
Indoxyl sulfate	N.S. by 5/6Nx, ↓ by AST-120	↑ by 5/6Nx, ↓ by AST-120	↑ in CKD patients	↑ in uremia	[8,19]
o-Hydroxybenzoate	N.S. by 5/6Nx, ↓ by AST-120		Not Detected		
Phenyl sulfate	NA	↑ by 5/6Nx, ↓ by AST-120	NA		
4-Ethylphenyl sulfate	NA	↑ by 5/6Nx, ↓ by AST-120	NA		
p-Cresyl sulfate	NA	↑ by 5/6Nx, ↓ by AST-120	NA		
Cationic compounds	**In this experiment**	**Repoted by Kikuchi *et al.* [9]**	**Reported in human by Toyohara T. *et al.* [13]**	**Others**	**References**
Gly	↑ by 5/6Nx, ↓ by AST-120		N.S.		
g-Guanidinobutyrate	↑ by 5/6Nx, ↓ by AST-120		N.S.	↑ in uremia	[19]
N-g-Ethylglutamine	↑ by 5/6Nx, ↓ by AST-120		Not Detected		
Allantoin	↑ by 5/6Nx, ↓ by AST-120		↑ in CKD patients	↑ in CKD patients	[20]